

1 **IL-11 neutralising therapies target hepatic stellate cell-induced liver**  
2 **inflammation and fibrosis in NASH**

3  
4

5 **Authors**

6 Anissa A. Widjaja<sup>1†</sup>, Brijesh K. Singh<sup>1†</sup>, Eleonora Adami<sup>1</sup>, Sivakumar Viswanathan<sup>1</sup>,  
7 Giuseppe A. D'Agostino<sup>1</sup>, Jinrui Dong<sup>1</sup>, Benjamin Ng<sup>1,2</sup>, Jessie Tan<sup>1,2</sup>, Bhairav S.  
8 Paleja<sup>3</sup>, Madhulika Tripathi<sup>1</sup>, Sze Yun Lim<sup>2</sup>, Sonia P. Chothani<sup>1</sup>, Wei Wen Lim<sup>1,2</sup>,  
9 Anne Rabes<sup>4</sup>, Martina Sombetzki<sup>4</sup>, Eveline Bruinstroop<sup>1</sup>, Rohit A. Sinha<sup>5</sup>, Salvatore  
10 Albani<sup>3</sup>, Paul M. Yen<sup>1</sup>, Sebastian Schafer<sup>1,2</sup>, Stuart A. Cook<sup>1,2,6,7\*</sup>

11  
12

13 **Affiliations**

14 <sup>1</sup>Cardiovascular and Metabolic Disorders Program, Duke–National University of Singapore  
15 Medical School, 169857, Singapore.

16 <sup>2</sup>National Heart Research Institute Singapore, National Heart Centre Singapore, 169609,  
17 Singapore.

18 <sup>3</sup>Translational Immunology Institute, SingHealth/Duke-NUS Academic Medical Centre,  
19 169856, Singapore.

20 <sup>4</sup>Department of Tropical Medicine and Infectious Diseases, University Medical Center,  
21 Rostock, 18057, Germany.

22 <sup>5</sup>Department of Endocrinology, Sanjay Gandhi Postgraduate Institute of Medical Sciences,  
23 Lucknow, 226014, India.

24 <sup>6</sup>National Heart and Lung Institute, Imperial College London, London, SW3 6LY, UK.

25 <sup>7</sup>MRC-London Institute of Medical Sciences, Hammersmith Hospital Campus, London, W12  
26 0NN, UK

27

28 \*Correspondence: S.A.C. ([stuart.cook@duke-nus.edu.sg](mailto:stuart.cook@duke-nus.edu.sg))

29 †These authors contributed equally to this work.

## 30 **Abstract**

31 The transformation of hepatic stellate cells (HSCs) into myofibroblasts is the defining  
32 pathobiology in non-alcoholic steatohepatitis (NASH). Here we show that key NASH  
33 factors induce IL-11, which drives an autocrine and ERK-dependent activation loop  
34 to initiate and maintain HSC-to-myofibroblast transformation, causing liver fibrosis.  
35 IL-11 is upregulated in NASH and *Il11ra1*-deleted mice are strongly protected from  
36 liver fibrosis, inflammation and steatosis in murine NASH. Therapeutic inhibition of  
37 IL11RA or IL-11 with novel neutralizing antibodies robustly inhibits NASH pathology  
38 in preclinical models and reverses established liver fibrosis by promoting HSC  
39 senescence and favourable matrix remodelling. When given early in NASH, IL-11  
40 inhibition prevents liver inflammation and steatosis, reverses severe hepatocyte  
41 damage and reduces hepatic immune cells and TGF $\beta$ 1 levels. Our findings show an  
42 unappreciated and central role for IL-11 in HSCs and prioritise IL-11 signalling as a  
43 new therapeutic target in NASH while revealing an unexpected pro-inflammatory  
44 function for IL-11 in stromal immunity.

## 46 **Introduction**

47 The global prevalence of nonalcoholic fatty liver disease (NAFLD) is estimated at  
48 25%<sup>1</sup> and while NAFLD is reversible it can progress to nonalcoholic steatohepatitis  
49 (NASH). NASH is characterized by steatosis-driven inflammation, hepatocyte death  
50 and liver fibrosis that can lead to liver failure. Hepatic stellate cells (HSCs) are pivotal  
51 in the pathogenesis of NASH and give rise to up to 95% of liver myofibroblasts<sup>2</sup>,  
52 which drive the key pathologies in NASH, namely liver fibrosis, inflammation and  
53 dysfunction<sup>3-5</sup>.

54  
55 A number of factors are implicated in HSC activation and transformation, including  
56 the canonical pro-fibrotic factors transforming growth factor- $\beta$ 1 (TGF $\beta$ 1) and platelet-  
57 derived growth factor (PDGF)<sup>6,7</sup> and also pro-inflammatory factors such as CCL2,  
58 TNF $\alpha$  and CCL5<sup>4,7,8</sup>. Perhaps reflecting this redundancy in HSC activation, no single  
59 upstream initiating factor has been targeted successfully in NASH. Inhibition of  
60 downstream pro-fibrotic targets such as LOXL2 has also been unsuccessful and  
61 ongoing clinical trials are focused mostly on inhibiting steatosis. There are no  
62 approved drugs for the treatment of NASH.

63  
64 Quiescent HSCs are vitamin A storing cells and very distinct from fibroblasts.  
65 However, common stimuli activate both cell types and stimulate their transition to  
66 myofibroblasts with shared features<sup>2,9</sup>. We recently identified Interleukin-11 (IL-11)  
67 as a crucial factor for cardiovascular and pulmonary fibroblast-to-myofibroblast  
68 transformation<sup>10,11</sup>. To date, there are very limited insights into IL-11 in the liver,  
69 where it is reported to have anti-inflammatory activity<sup>12,13</sup>, and it is unknown if HSCs  
70 respond to IL-11 at all. Here, we explore the hypothesis that IL-11 plays a role in the  
71 transformation of HSCs into myofibroblasts and determine the effects IL-11 signalling  
72 in the context of liver inflammation, steatosis and fibrosis in NASH.

## 74 **IL-11 activates HSCs and drives liver fibrosis in NASH**

75 Genome wide RNA-seq analysis revealed that TGF $\beta$ 1 strongly upregulates *IL-11*  
76 (14.9-fold,  $P = 3.40 \times 10^{-145}$ ) in HSCs that was confirmed by qPCR and at the protein  
77 level and replicated in experiments using precision cut human liver slices (**Fig. 1a-c**,  
78 **Supplementary Fig. 1a**). Independent RNA-seq data<sup>14</sup> also show that *IL-11* is the  
79 most upregulated gene in HSCs when grown on a stiff substrate to model cirrhotic

80 liver (**Supplementary Fig. 1b**). HSCs express very low levels of IL6R and higher  
81 levels of the IL-11 receptor subunit alpha (IL11RA) than either cardiac or lung  
82 fibroblasts (**Fig. 1d, Supplementary Fig. 1c**). We also performed Western blots on  
83 patient liver samples and found increased IL-11 levels in NASH (**Supplementary**  
84 **Fig. 1d,e**). These data show that HSCs are both a source and prominent target of IL-  
85 11 in the human liver and that IL-11 is elevated in NASH.

86

87 To investigate the effect of IL-11 on HSCs, we stimulated cells with either IL-11,  
88 TGF $\beta$ 1 or PDGF. IL-11 activated HSCs to a similar extent as TGF $\beta$ 1 or PDGF,  
89 transforming quiescent HSCs into ACTA2<sup>+ve</sup> myofibroblasts that secrete collagen  
90 and matrix modifying enzymes (**Fig. 1e-g, Supplementary Fig. 1f**). IL-11 also  
91 promoted dose-dependent matrix invasion by HSCs that is an important aspect of  
92 HSC pathobiology in NASH (**Fig. 1h**). We stimulated HSCs with hyperIL-11<sup>10</sup> to  
93 test for an autocrine loop of feed-forward IL-11 activity, inferred by IL-11 secretion  
94 from HSCs that express IL11RA, and confirmed its existence (**Fig. 1i**). Moving *in*  
95 *vivo*, subcutaneous administration of recombinant mouse Il-11 (rml-11) to mice for  
96 21 days increased hepatic collagen content, fibrosis marker mRNA and serum  
97 alanine aminotransferase (ALT) levels (**Fig. 1j-m**). Furthermore, *Col1a1-GFP*  
98 reporter mice<sup>15</sup> treated with rml-11 accumulated *Col1a1*<sup>+ve</sup> myofibroblasts in the liver  
99 (**Supplementary Fig. 1g**).

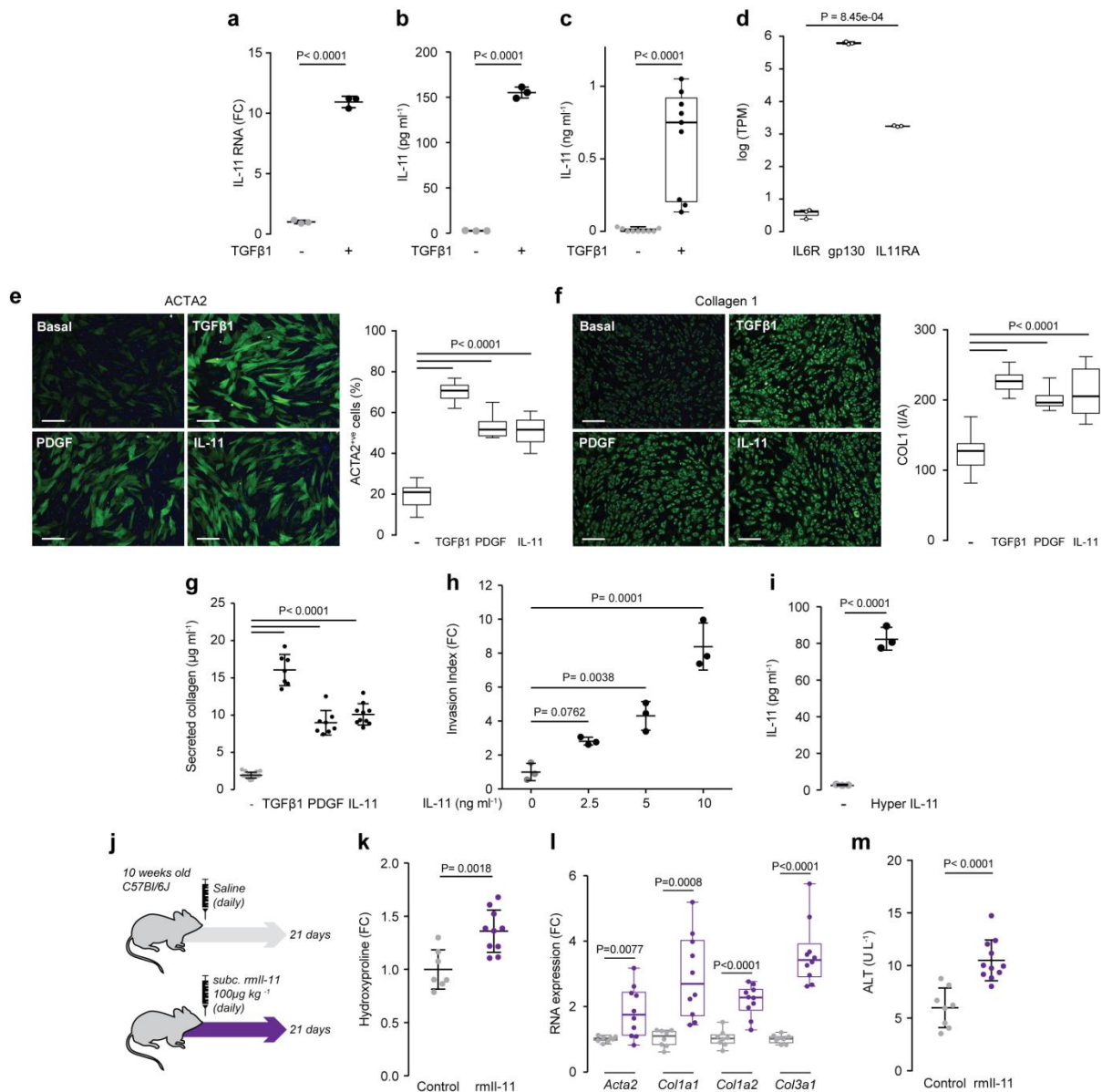


**Figure 1. IL-11 induces hepatic stellate cell activation and hepatic fibrosis.**

100  
 101  
 102  
 103 **a**, IL-11 is upregulated in hepatic stellate cells (HSCs) stimulated with TGFβ1 (n=3). **b**, IL-11 protein is  
 104 secreted from HSCs stimulated with TGFβ1 (ELISA, n=3). **c**, Human precision cut liver slices were  
 105 stimulated with TGFβ1 and IL-11 protein was measured in supernatant (ELISA, n=3). **d**, IL6R, gp130,  
 106 and IL11RA expression in HSCs (TPM, transcripts per million). **e**, **f**, Representative fluorescence  
 107 images (scale bars, 200 μm) of HSCs and automated fluorescence quantification for **(e)** ACTA2<sup>+</sup>ve  
 108 cells and **(f)** Collagen I immunostaining following incubation without stimulus (-), with TGFβ1, PDGF,  
 109 or IL-11. **g**, Collagen secretion supernatants of HSC stimulated with TGFβ1, PDGF, or IL-11 (Sirius  
 110 red assay. n≥7). **h**, Dose-dependent matrigel invasion of HSCs induced by IL-11(n=3). **i**, Hyper IL-11  
 111 induces IL-11 protein secretion from HSCs (ELISA, n=3). **a-c**, **e-g**, **i**, TGFβ1 (5 ng ml<sup>-1</sup>), Hyper IL-11  
 112 (0.2 ng ml<sup>-1</sup>), PDGF (20 ng ml<sup>-1</sup>), IL-11 (5 ng ml<sup>-1</sup>); 24 h stimulation; **h**, 48 h stimulation. **j**, Schematic of  
 113 mice receiving daily subcutaneous injection of either saline (control) or rml-11 (100 μg kg<sup>-1</sup>). **k**,  
 114 Relative liver hydroxyproline content, **l**, mRNA expression of pro-fibrotic markers, and **m**, serum ALT  
 115 levels (**k**, **l**, control, n=7; rml-11, n=10; **m**, control n=8; rml-11, n=11). **a**, **b**, **g**, **h**, **i**, **k**, **m** Data are  
 116 represented as mean ± s.d.; **c-f**, **l**, Box-and-whisker plots show median (middle line), 25th–75th  
 117 percentiles (box) and min-max percentiles (whiskers). **a-d**, **i**, **k-m**, Two-tailed Student's *t*-test; **e-h**,  
 118 two-tailed Dunnett's test. FC: fold change; I/A: intensity/area.

## 119 **Anti-IL-11 therapies are effective in treating murine NASH**

120 We next performed studies in a murine model of severe NASH using the high fat  
121 methionine- and choline-deficient (HFMCD) diet<sup>16</sup>. In this model, *Il-11* mRNA was  
122 mildly elevated whereas protein levels were highly upregulated, revealing strong  
123 post-transcriptional regulation of Il-11 expression in the liver (**Supplementary Fig.**  
124 **2a,b**). The progressive induction of Il-11 protein was mirrored by ERK activation,  
125 increased collagen and elevated serum ALT levels (**Fig. 2a-c, Supplementary Fig.**  
126 **2c**). To evaluate the physiological relevance of increased Il-11 levels in NASH, we  
127 used a genetic loss-of-function model: the Il-11 receptor subunit alpha deleted  
128 mouse (*Il11ra1<sup>-/-</sup>*)<sup>17</sup>. *Il11ra1<sup>-/-</sup>* mice on the NASH diet were protected from fibrosis and  
129 had lesser steatosis and liver damage and ERK activation (**Fig. 2d-g,**  
130 **Supplementary Fig. 2d,e**). Hence, non-canonical and ERK-dependent Il-11  
131 signalling, seen previously during fibroblasts-to-myofibroblast transformation<sup>10</sup>,  
132 appeared relevant for several distinct aspects of NASH pathobiology.

133

134 In an attempt to target the IL-11 autocrine loop, we genetically immunised mice with  
135 IL11RA to generate neutralising anti-IL11RA antibodies. Clones that block fibroblast  
136 transformation<sup>10</sup> were identified and clone X209 (IgG1 $\kappa$ ,  $K_D = 6$ nM) that neutralised  
137 IL-11 signalling across species was prioritised. X209 blocked fibrogenic protein  
138 secretion from HSCs with an  $IC_{50}$  of 5.4pM. Pharmacokinetic studies using <sup>125</sup>I-X209  
139 revealed an *in vivo* half-life of more than 18 days and strong uptake in the liver  
140 (**Supplementary Fig. 3**). To ensure therapeutic specificity for IL-11 signalling and  
141 exclude off-target effects, we also developed a neutralising anti-IL-11 antibody  
142 (X203)<sup>11</sup> and used both antibodies in downstream studies.

143

144 Initial experiments revealed that both antibodies blocked the TGF $\beta$ 1-driven transition  
145 of HSCs into myofibroblasts (**Fig. 2h, Supplementary Fig. 4a,b,d,e,g**). Follow on  
146 studies found that other key NASH stimuli such as PDGF, CCL2, angiotensin II,  
147 bFGF or oxidative stress also induce IL-11 secretion from HSCs. And, remarkably,  
148 HSC-to-myofibroblast transformation downstream of these various stimuli is  
149 consistently dependent on intact IL-11 signalling (**Fig. 2i-k, Supplementary Fig.**  
150 **4c,f,h,i**). Thus, IL-11 activity is a critical and universal feature underlying HSC  
151 transformation, which has similarities with its activity in fibroblasts<sup>10,11</sup>.

152

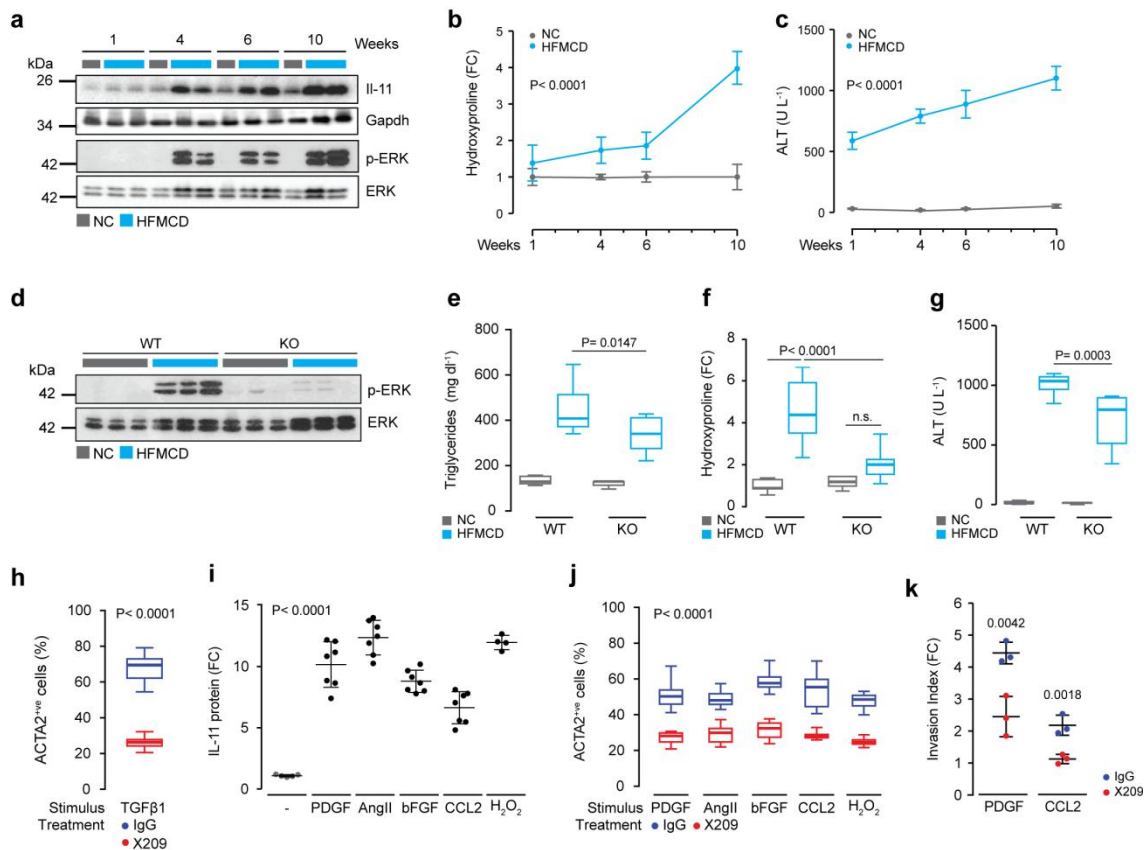
153 We then tested X209 and X203 therapy *in vivo* and started antibody administration  
154 (10 mg kg<sup>-1</sup> bi-weekly) after six weeks of NASH diet when IL-11 is strongly  
155 upregulated, collagen has accumulated and there is severe steatohepatitis (**Fig. 2a-**  
156 **c, 3a, Supplementary Fig. 5a**). After four weeks of therapy both antibodies had  
157 abolished ERK activation, demonstrating excellent target engagement and coverage.  
158 Anti-IL-11 therapies inhibited the progression in liver fibrosis and serum ALT levels,  
159 while steatosis was largely unchanged (**Fig. 3b-e, Supplementary Fig. 5b-g**).

160

161 To extend these findings, we tested anti-IL-11 therapy in an additional NASH model  
162 using obese and insulin resistant (*db/db*) mice on a methionine- and choline-deficient  
163 (MCD) diet (**Fig. 3f**)<sup>18-20</sup>. As expected, Il-11 expression and ERK activation were  
164 increased in livers of MCD fed *db/db* mice (**Fig. 3g,h**). Furthermore, anti-IL11  
165 therapy reduced hepatic steatosis, fibrosis, inflammation and improved ALT levels as  
166 compared to controls (**Fig. 3i-m, Supplementary Fig. 6a**). A third model of  
167 streptozotocin-induced diabetes and advanced NASH (**Supplementary Fig. 6b**) was  
168 investigated although ALT was not elevated in this model at tissue collection,



169 perhaps reflecting end-stage disease (**Supplementary Fig. 6c**). Nonetheless, levels  
 170 of fibrosis and inflammation genes were robustly inhibited by either X203 or X209  
 171 therapy in this third model (**Supplementary Fig. 6d,e**).  
 172



173  
 174

**Figure 2. Inhibition of IL-11 signaling prevents hepatic stellate cell activation and hepatic fibrosis**

175  
 176  
 177 **a**, Western blots of hepatic IL-11 and ERK activation status in mice on HFMCD diet. **b**, Relative liver  
 178 hydroxyproline content and **c**, serum ALT levels in mice fed on HFMCD diet; liver tissues and serum  
 179 were collected at the indicated time points (NC 1, 4, 6 week(s), n=5; NC HPA 10 weeks, n=4; NC ALT  
 180 10 weeks, n=5; HFMCD 1 week, n=7; HFMCD 4, 6 weeks, n=8; HFMCD 10 weeks, n=5). **d**, Western  
 181 blots of hepatic ERK activation status after 10 weeks of HFMCD diet in *Il11ra*<sup>+/+</sup> (WT) and *Il11ra*<sup>-/-</sup>  
 182 (KO) mice. **e**, Liver triglyceride levels and **f**, relative liver hydroxyproline content in WT and KO mice  
 183 fed with HFMCD diet for 10 weeks (NC WT, n=9; HFMCD WT, n=9; NC KO, n=5; HFMCD KO, n=9).  
 184 **g**, Serum ALT levels in WT and KO mice following HFMCD diet (NC WT, n=9; HFMCD WT, n=8; NC  
 185 KO, n=5; HFMCD KO, n=9). **h**, ACTA2<sup>ve</sup> cells numbers in hepatic stellate cell (HSC) cultures  
 186 stimulated with TGFβ1 in the presence of either IgG or X209. **i**, ELISA of IL-11 secretion from HSCs  
 187 stimulated with various NASH factors (basal, n=5; PDGF, AngII, bFGF, CCL2, n=7; H<sub>2</sub>O<sub>2</sub>, n=4). **j**,  
 188 Effect of X209 on ACTA2<sup>ve</sup> cell proportions in HSCs stimulated with various NASH factors. **k**, Effects  
 189 of X209 on PDGF- or CCL2-induced HSC invasion (n=3). **h, j**, 24 h stimulation; **i, k**, 48 h stimulation.  
 190 **h-k**, TGFβ1 (5 ng ml<sup>-1</sup>), Hyper IL-11 (0.2 ng ml<sup>-1</sup>), PDGF (20 ng ml<sup>-1</sup>), AngII (100 nM), bFGF (10 ng  
 191 ml<sup>-1</sup>), CCL2 (5 ng ml<sup>-1</sup>), H<sub>2</sub>O<sub>2</sub> (0.2 mM), IgG and X209 (2 μg ml<sup>-1</sup>). **b, c, i, k**, Data are represented as  
 192 mean ± s.d.; **e-h, j**, data are shown as box-and-whisker with median (middle line), 25th–75th  
 193 percentiles (box) and min-max percentiles (whiskers). **b, c**, Two-way ANOVA; **e-g**, two-tailed, Sidak-  
 194 corrected Student's *t*-test; **h-k**, two-tailed Dunnett's test. FC: fold change; NC: normal chow; HFMCD:  
 195 high fat methionine- and choline-deficient.

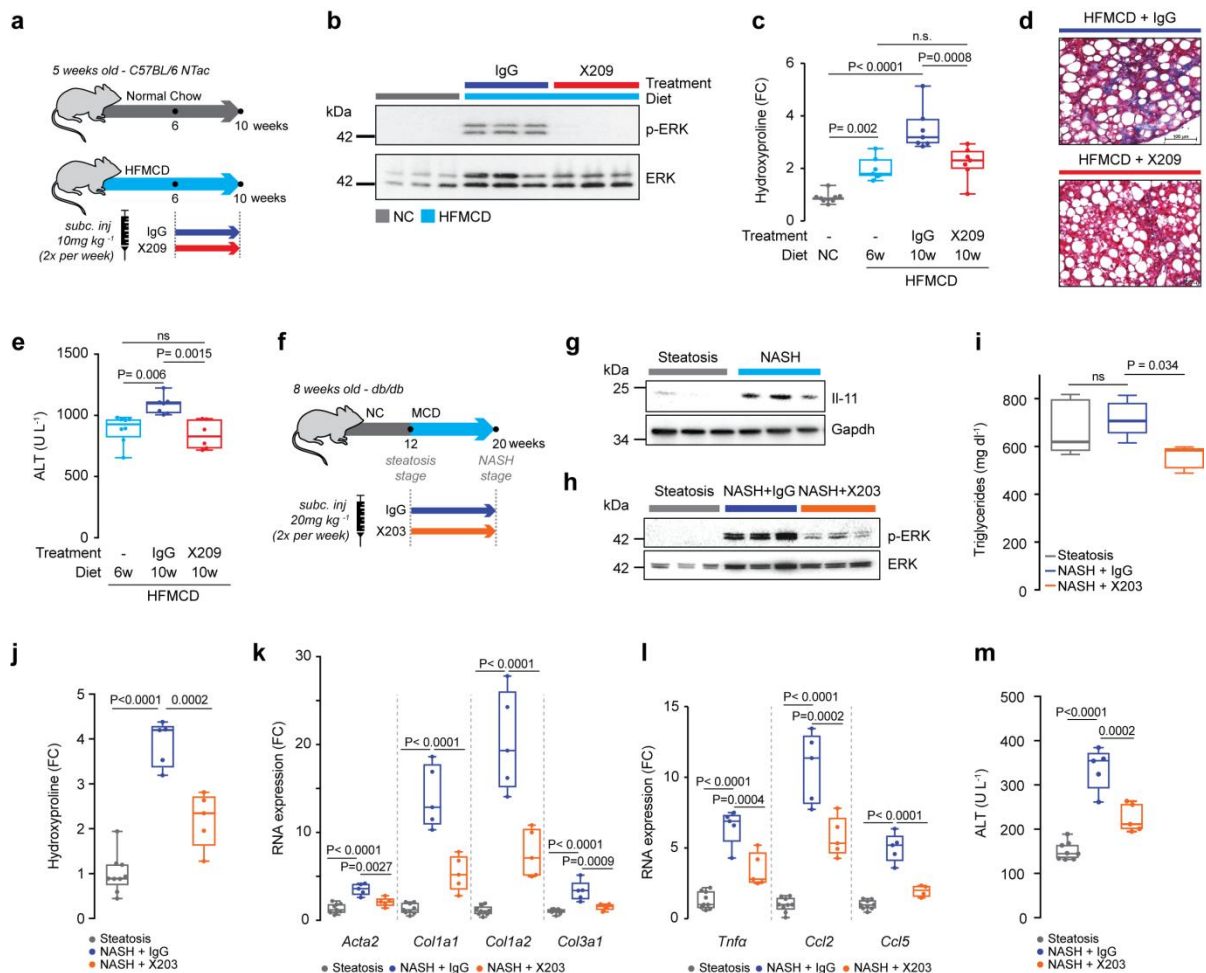


**Figure 3. Therapeutic inhibition of IL-11 signalling inhibits the progression of late stage NASH**

**a**, Schematic showing therapeutic use of X209 in HFMCD-fed mice. X209 or IgG isotype control ( $10 \text{ mg kg}^{-1}$ , twice a week) were administered from week 6 to 10 of HFMCD diet. **b-e**, Data for therapeutic dosing experiments as shown in **3a**. **b**, Western blots of hepatic ERK activation status. **c**, Relative liver hydroxyproline content (NC, n=9; HFMCD 6 weeks, n=8; IgG, n=8; X209, n=9; the values of NC and HFMCD 6 weeks are the same as those used in **2b**). **d**, representative Masson's Trichrome staining, **e**, serum ALT levels (HFMCD 6 weeks, n=8; IgG, n=7; X209, n=6; the values of HFMCD 6 weeks are the same as those used in **2c**) of X209- and IgG- treated mice. **f**, Schematic of X203 or IgG administration to MCD-fed *db/db* mice and times of liver sample collection for use in experiments shown in **g-m**. **g**, Western blots of hepatic IL-11 and Gapdh. **h**, Western blots of total and phosphorylated ERK levels in livers of X203 or IgG- treated mice. **i**, Hepatic triglyceride content, **j**, liver hydroxyproline content, and **k**, pro-fibrotic and **l**, pro-inflammatory mRNA expression (steatosis, n=9; NASH+IgG, n=5; NASH+X203, n=5). **m**, Serum ALT levels (steatosis, n=8; NASH+IgG, n=5; NASH+X203, n=5). **c**, **e**, **i-m**, Data are shown as box-and-whisker with median (middle line), 25th–75th percentiles (box) and min-max percentiles (whiskers); two-tailed, Tukey-corrected Student's *t*-test. FC: fold change; NC: normal chow; HFMCD: high fat methionine- and choline-deficient; MCD: methionine- and choline-deficient.

### Neutralisation of IL-11 signalling reverses hepatic fibrosis

While inhibition of IL-11 signalling in mice on HFMCD diet did not reverse total hepatic collagen protein content, there was reversal of *Col1a1*, *Timp1*, and *Tgfb1* RNA expression (**Supplementary Fig. 5g**). To test more fully, if IL-11 inhibition can reverse the fibrotic phenotype beyond the RNA level, we first established severe liver fibrosis and then removed the fibrogenic stimulus and started antibody treatment (**Fig. 4a**). Hepatic collagen content was significantly reversed after three weeks of X203 or X209 treatment and even greater reversal was seen at 6 weeks (**Fig. 4b**,

196

197

198

199

200

201

202

203

204

205

206

207

208

209

210

211

212

213

214

215

216

217

218

219

220

221

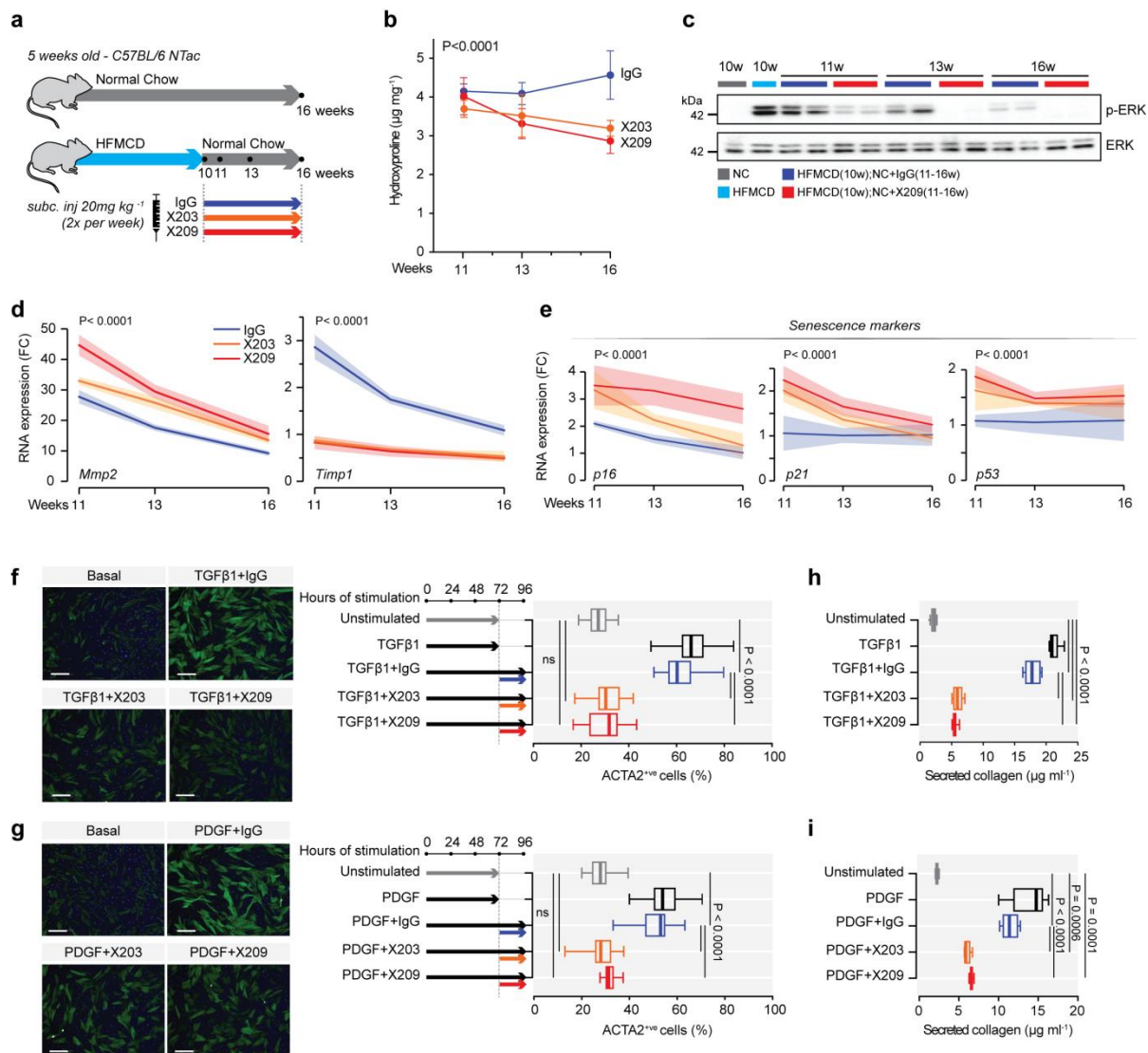
222

223

224 **Supplementary Fig. 7a**). In the absence of the dietary trigger, ERK activation  
225 spontaneously regressed, which was accelerated by X203 or X209-treatment.  
226 Notably, collagen content remained unchanged in IgG control-treated animals for the  
227 duration of the experiment (**Fig. 4c, Supplementary Fig. 7b**). As such, anti-IL-11  
228 therapies reverse liver fibrosis but this effect is limited in the context of active and  
229 severe steatosis where combination therapy with an anti-steatotic may be more  
230 effective.

231  
232 Regression of liver fibrosis is associated with lower TIMP and higher MMP levels,  
233 which promotes favorable matrix remodelling<sup>3,21</sup>. In keeping with this, X203 or X209  
234 treated mice rapidly exhibited strong upregulation of *Mmp2* and marked  
235 downregulation of *Timp1* (**Fig. 4d**). Reversal of hepatic fibrosis is favoured when  
236 transformed HSCs undergo apoptosis<sup>22</sup>, senescence<sup>23,24</sup> or reversion to an inactive,  
237 ACTA2<sup>-ve</sup> cellular state<sup>25</sup>. We examined these potential mechanisms and found  
238 decreased *Acta2*, increased senescence markers (*p21*, *p16*, and *p53*) but no change  
239 in apoptosis factors with anti-IL-11 therapies (**Fig. 4e, Supplementary Fig. 7c,d**). To  
240 check directly if IL-11 signalling is required to maintain HSCs in a transformed state,  
241 we stimulated HSCs with TGF $\beta$ 1 or PDGF and then inhibited IL-11 signalling in the  
242 presence of ongoing stimulation. Within 24 h of IL-11 inhibition, the percentage of  
243 ACTA2<sup>+ve</sup> cells and the amount of secreted collagen were reversed to near baseline  
244 levels, as was ERK activity (**Fig. 4f-i, Supplementary Fig. 7e,f**). These data show  
245 that inhibition of IL-11-dependent HSC transformation causes HSC  
246 senescence/reversion and favorable matrix remodelling leading to fibrosis  
247 regression.





248  
249

**Figure 4. Therapeutic inhibition of IL-11 signalling reverses HSC transformation and liver fibrosis.**

**a**, Schematic showing reversal experiment with X203 or X209. Fibrosis was established by feeding mice the NASH diet for 10 weeks and then replacing this with normal chow (NC) and initiating antibody (X203 and X209) therapy. Mice were euthanised at the indicated time points. **b-e**, Data for therapy experiments as shown in **4a**. **b**, Total liver hydroxyproline content, **c**, western blots of hepatic ERK activation status, **d**, relative mRNA expression of *Mmp2* and *Timp1*, and **e**, senescence markers at 1-, 3-, 6-weeks after X203, X209, or IgG treatment (n≥3/group). **f, g**, Automated fluorescence quantification and representative fluorescence images of ACTA2<sup>+</sup> immunostaining (scale bars, 200 µm) following incubation without stimulus (-), (**f**) with TGFβ1, (**g**) with PDGF, either prior to or after the addition of X203, X209, or IgG. **h, i**, The amount of collagen secreted by HSCs stimulated with (**h**) TGFβ1 or (**i**) PDGF either prior to or after the addition of IgG, X203, or X209 (n=5/group). **f-i**, TGFβ1 (5 ng ml<sup>-1</sup>), PDGF (20 ng ml<sup>-1</sup>), IgG, X203 and, X209 (2 µg ml<sup>-1</sup>). **b**, Data are shown as mean ± s.d; **d**, **e**, data are represented as line chart (mean) and transparencies indicate s.d; **f-i**, data are shown as box-and-whisker with median (middle line), 25th–75th percentiles (box) and min-max percentiles (whiskers). **b, d, e**, Two-way ANOVA; **f-i**, Two-tailed, Tukey-corrected Student's *t*-test. FC: fold change; NC: normal chow; HFMC: high fat methionine- and choline-deficient.

266

## 267 **Blocking IL-11 signalling inhibits liver inflammation in NASH**

268 Beyond their role in liver fibrosis, HSCs have a central role in hepatic inflammation  
269 through the secretion and paracrine activity of pro-inflammatory cytokines and  
270 chemokines<sup>3,8,26,27</sup>. We profiled inflammatory gene expression in NASH livers from  
271 *Il11ra1*<sup>-/-</sup>, X203- or X209-treated mice and observed consistently lower levels of  
272 *TNF $\alpha$* , *CCL2* and *CCL5* with IL-11 loss-of-function when compared to experimental  
273 controls (**Supplementary Fig. 8a,b**). We determined if these effects on inflammation  
274 *in vivo* were related to the action of IL-11 on HSCs and found that IL-11 stimulated  
275 HSC secretion of CCL2 whereas IL-11 inhibition blocked CCL2 secretion  
276 (**Supplementary Fig. 8c**). This reveals an unappreciated role for IL-11 in stromal  
277 immunity and shows that IL-11 neutralisation inhibits paracrine effects of pro-  
278 inflammatory factors secreted from HSCs on other cells in the hepatic niche<sup>3,8,26,27</sup>.

279

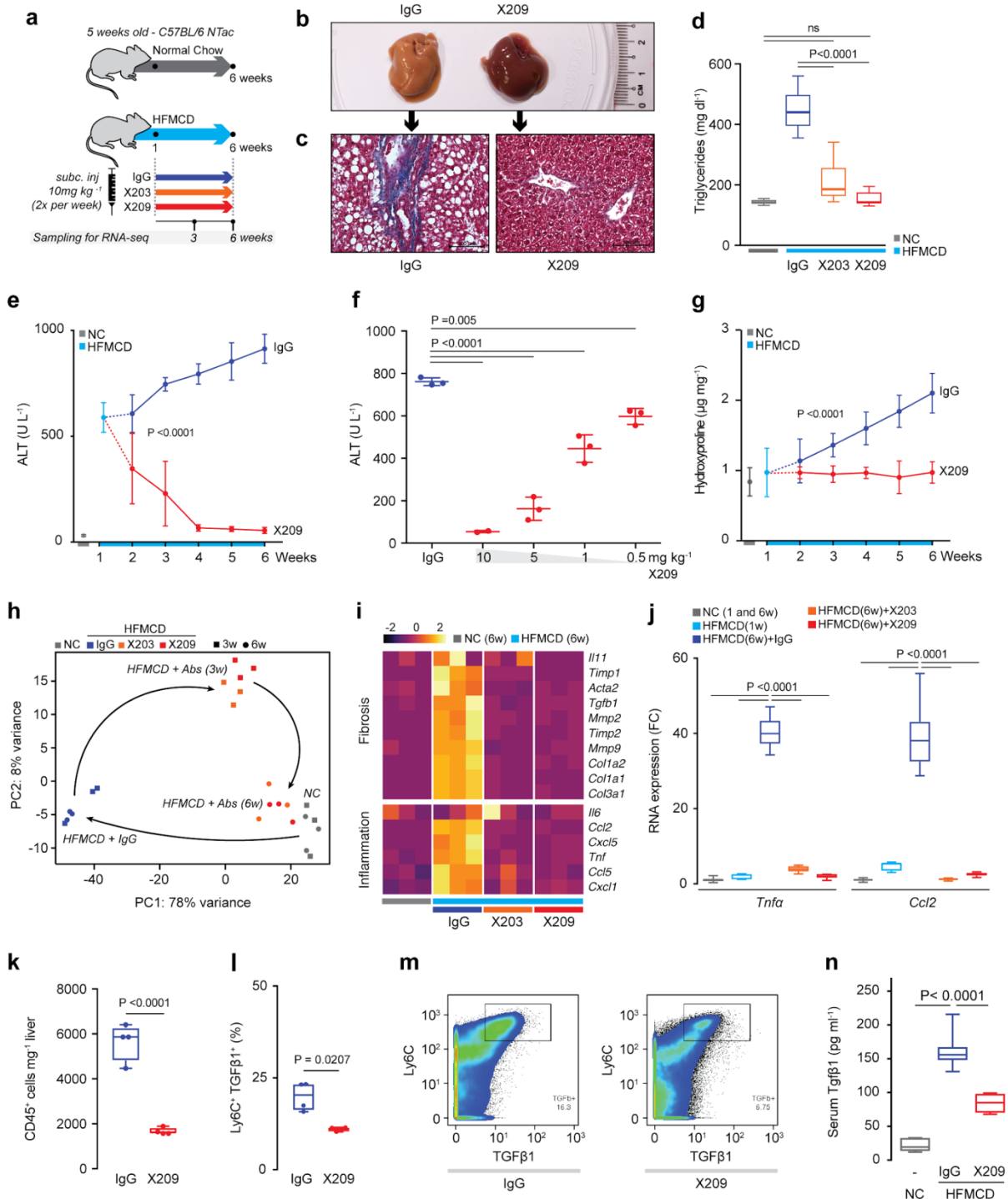
280 In the HFMCD diet model of NASH, inflammation peaks at six weeks and is then  
281 followed by a phase of severe fibrosis (**Supplementary Fig. 8d**). We inhibited IL-11  
282 signalling early during steatohepatitis and found that livers of X203- and X209-  
283 treated mice were strikingly less steatotic and had lesser ERK activation (**Fig. 5a,b**,  
284 **Supplementary Fig. 8e-g**). At the molecular level, there was a significant reduction  
285 in triglyceride content and lipid droplets in hepatocytes of X203- and X209-treated  
286 mice were not apparent (**Fig. 5c,d**, **Supplementary Fig. 8h**). HFMCD diet induces  
287 marked steatohepatitis and liver damage after one week (ALT>700 U L<sup>-1</sup>), which was  
288 reversed in a dose-dependent manner to near normal after three weeks of either  
289 X203 or X209 treatment (**Fig. 5e,f**, **Supplementary Fig. 8i**). As expected, X203 or  
290 X209 treated mice did not develop fibrosis during the experiment, reaffirming the  
291 strong anti-fibrotic effects associated with inhibition of IL-11 signaling (**Fig. 5c,g**,  
292 **Supplementary Fig. 8h,j,k**).

293

294 We next performed RNA-seq to profile globally the effects of IL-11 inhibition during  
295 steatohepatitis. Unsupervised analyses of these data showed that antibody  
296 treatment almost completely reverses the pathological RNA expression signature  
297 induced by HFMCD diet (**Fig. 5h**, **Supplementary Fig. 9a,b**). Upregulation of pro-  
298 fibrotic and pro-inflammatory genes was abolished and lipid metabolism gene  
299 expression re-established by anti-IL11RA therapy (**Fig. 5i,j**, **Supplementary Fig. 9c-**  
300 **e**). Unbiased Gene Set Enrichment Analyses confirmed the reversion of HFMCD  
301 diet-induced changes in metabolic and inflammatory transcriptional signatures  
302 (**Supplementary Fig. 10**).

303

304 Resident macrophages and infiltrating monocytes are important for NASH  
305 pathogenesis and a major source of TGF $\beta$ 1 during disease progression<sup>28</sup>. We  
306 examined inflammatory cell populations in the liver during steatohepatitis and  
307 observed fewer immune cells in general in X209-treated livers and a specific  
308 reduction in Ly6C<sup>+ve</sup>TGF $\beta$ 1<sup>+ve</sup> cells (**Fig. 5k-m**). TGF $\beta$ 1 is a major determinant of  
309 fibrosis in NASH and can be produced by Kupffer, HSCs and other cells in the liver<sup>5</sup>.  
310 Circulating TGF $\beta$ 1 levels were elevated by HFMCD diet but reduced by X209  
311 therapy, which shows that anti-IL11RA therapy is disease-modifying (**Fig. 5n**).



312  
313  
314  
315  
316  
317  
318  
319  
320  
321  
322  
323  
324

### Figure 5: Neutralisation of IL-11 signalling reverses liver damage in early stage NASH.

**a**, Schematic of the anti-IL11 therapy experiment early on in the HFMCD diet NASH model. Antibody treatments were started 1 week after the start of NASH diet when X209, X203, or IgG control (10 mg kg<sup>-1</sup>, twice a week) were administered intraperitoneally for 5 weeks. **b-n**, Data for experiments as shown in **5a**. **b**, Representative gross liver images and **c**, representative Masson's Trichrome stained images of livers after 5 weeks of IgG or X209 treatments. **d**, Hepatic triglyceride levels (NC, n=5; IgG, n=14; X203, n=10; X209, n=8). **e**, Serum ALT levels (n≥5/group, the values of NC and HFMCD 1 week are the same as those used in **2c**). **f**, Dose-dependent effect of 3-week X209 therapy on reversal of serum ALT levels (n=3/group). **g**, Liver hydroxyproline content of X209- or control IgG-treated mice (n≥5/group, the values of NC and HFMCD 1 week are the same as those used in **Fig. 2b**). **h**, Principal component analysis (PCA) plot of liver gene expression in mice on NC or HFMCD in

325 the presence of IgG, X203 or X209 antibodies for the times shown in **5a** (RNA-seq, n=3/group).  
326 Arrows depict the transitions from normal gene expression (NC) to most perturbed gene expression in  
327 NASH (HFMCD+IgG), to intermediately restored gene expression (HFMCD+Abs (3w)), to normalised  
328 gene expression (HFMCD+Abs(6w)) **i**, Differential expression heatmap of pro-fibrotic and pro-  
329 inflammatory genes Z-scores (Transcripts Per Million mapped reads, TPM). **j**, *Tnfa* and *Ccl2* mRNA  
330 expression by qPCR (NC, n=9; HFMCD 1 week, n=7; IgG, n=14; X203, n=10; X209, n=8). **k**, Liver  
331 CD45<sup>+ve</sup> immune cell numbers, **l**, Ly6C<sup>+ve</sup> TGFβ1<sup>+ve</sup> cells in the total CD45<sup>+ve</sup> populations and **m**,  
332 representative pseudocolor plots illustrating the gating strategy used to detect Ly6C<sup>+ve</sup> TGFβ1<sup>+ve</sup> cells.  
333 **k-m**, (n=4/group). **n** Serum TGFβ levels (NC, n=5; IgG, n=14; X203, n=10; X209, n=8). **d, j, k, l, n**,  
334 Data are shown as box-and-whisker with median (middle line), 25th–75th percentiles (box) and min-  
335 max percentiles (whiskers); **e-g**, data are shown as mean ± s.d. **d, j, n**, Two-tailed, Tukey-corrected  
336 Student's *t*-test; **e, g**, two-way ANOVA; **f**, two-tailed Dunnett's test; **k, l**, two-tailed Student's *t*-test. FC:  
337 fold change; NC: normal chow; HFMCD: high fat methionine- and choline-deficient.  
338

## 339 Discussion

340 Recognition of HSCs as the major source for myofibroblasts in the liver<sup>2</sup> prioritizes  
341 their transformation as a specific and fundamental target in fibrotic liver diseases.  
342 We have previously identified an important function of IL-11 for cardiac and renal  
343 fibroblast-to-myofibroblast transformation<sup>10</sup>. We reveal here that IL-11 has non-  
344 redundant signalling activity required for HSC activation and transformation, which is  
345 positioned at a decisive intersection of several pathogenic pathways. Our findings  
346 show that non-canonical IL-11 signalling is an overlooked and cardinal process for  
347 myofibroblast generation from both fibroblasts and HSCs, and likely pericytes and  
348 other cell types, and confirm a key role for ERK signaling in hepatic fibrosis<sup>29</sup>.

349  
350 The multi-faceted pathobiology of HSCs touches upon many aspects of liver  
351 disease: fibrosis, metabolism, immunoregulation and secretion of paracrine factors in  
352 the hepatic niche<sup>3</sup>. Confirming the central role of IL-11 for HSC pathobiology, our  
353 first-in-class IL-11 neutralising treatments show disease-modifying therapeutic  
354 impact beyond anti-fibrotic effects alone. Inhibition of IL-11 signaling prevents  
355 inflammation and steatosis and can reverse liver fibrosis and hepatocyte damage.  
356 Unlike steatosis, fibrosis in NASH predicts clinical endpoints and anti-fibrotic IL-11  
357 blocking therapies may offer benefits over drugs that primarily target liver  
358 metabolism<sup>1</sup>.

359  
360 While earlier publications suggest IL-11 is anti-inflammatory in liver<sup>12,13</sup>, these  
361 studies use high-dose recombinant human IL-11 in the mouse, where effects can be  
362 non-specific<sup>10</sup>. In contrast, we show here that the biological effect of endogenous IL-  
363 11 at physiological levels is the opposite: HSC-immune cell crosstalk and activation  
364 is IL-11 dependent and inhibition of IL-11 is anti-inflammatory and cytoprotective.  
365 Our study demonstrates robust modulation of the immune response by targeting  
366 stromal cells through IL-11 inhibition, which was unexpected. This may have  
367 implications for other fibro-inflammatory processes where stromal and immune cell  
368 functions are closely interlinked, as in tumour microenvironments<sup>30,31</sup> and  
369 autoimmune diseases<sup>32,33</sup>.

370  
371 Human<sup>34</sup> and mouse<sup>17</sup> knockouts of *IL11RA* have mild developmental abnormalities  
372 of the skull but are otherwise healthy and IL-11 appears largely redundant in adult  
373 mammals. This provides compelling genetic safety data for IL-11 as a viable drug  
374 target and we suggest that IL-11 neutralising therapies should be evaluated in  
375 NASH. This is the first study to demonstrate a role for IL-11 in HSC biology, NASH or  
376 stromal immunity and lays the groundwork for future studies to dissect fully the



377 effects of IL-11 signaling in the liver. We believe this presents an exciting opportunity  
378 and that our findings may have broad implications across tissues and diseases.  
379

### 380 **Acknowledgements**

381 The authors would like to acknowledge the technical expertise and support of N.S-  
382 J.Ko, B.L.George, M. Wang, and NGS Team at NHCS. The research was supported  
383 by the National Medical Research Council (NMRC) Singapore STaR awards to  
384 S.A.C. (NMRC/STaR/0029/2017), the NMRC Central Grant to the NHCS, Goh  
385 Foundation, Tanoto Foundation and a grant from the Fondation Leducq. A.A.W. is  
386 supported by the NMRC YIRG (NMRC/OFYIRG/0053/2017). B.K.S. is supported by  
387 the NMRC YIRG (NMRC/OFYIRG/0002/2016). P.M.Y. is supported by  
388 NMRC/CSA/0054/2013 and NMRC/CIRG/1457/2016.

389

### 390 **Author contributions**

391 A.A.W., B.K.S., S.S., and S.A.C. conceived and designed the study. A.A.W., B.K.S.,  
392 S.V., J.R.D., B.N., J.T., and M.T. performed *in vitro* cell culture, cell biology and  
393 molecular biology experiments. A.A.W., B.K.S., J.T., M.T., A.R., M.S., E.B., and  
394 R.A.S. performed *in vivo* gain- and loss-of function mouse studies. N.G-C. and  
395 S.M.E. performed gain-of function studies on *Col1a1-GFP* mice. A.A.W., W.W.L.,  
396 and S.Y.L. performed histology analysis. A.A.W and S.V. performed *in vitro* antibody  
397 screening. G.D., S.P.C., and S.S performed computational analysis. B.S.P and S.A.  
398 performed CyTOF. A.A.W., B.K.S, E.A., G.D., B.N., R.A.S., P.M.Y., S.S., and S.A.C  
399 analyzed the data. A.A.W., E.A., S.S., and S.A.C prepared the manuscript with input  
400 from co-authors.

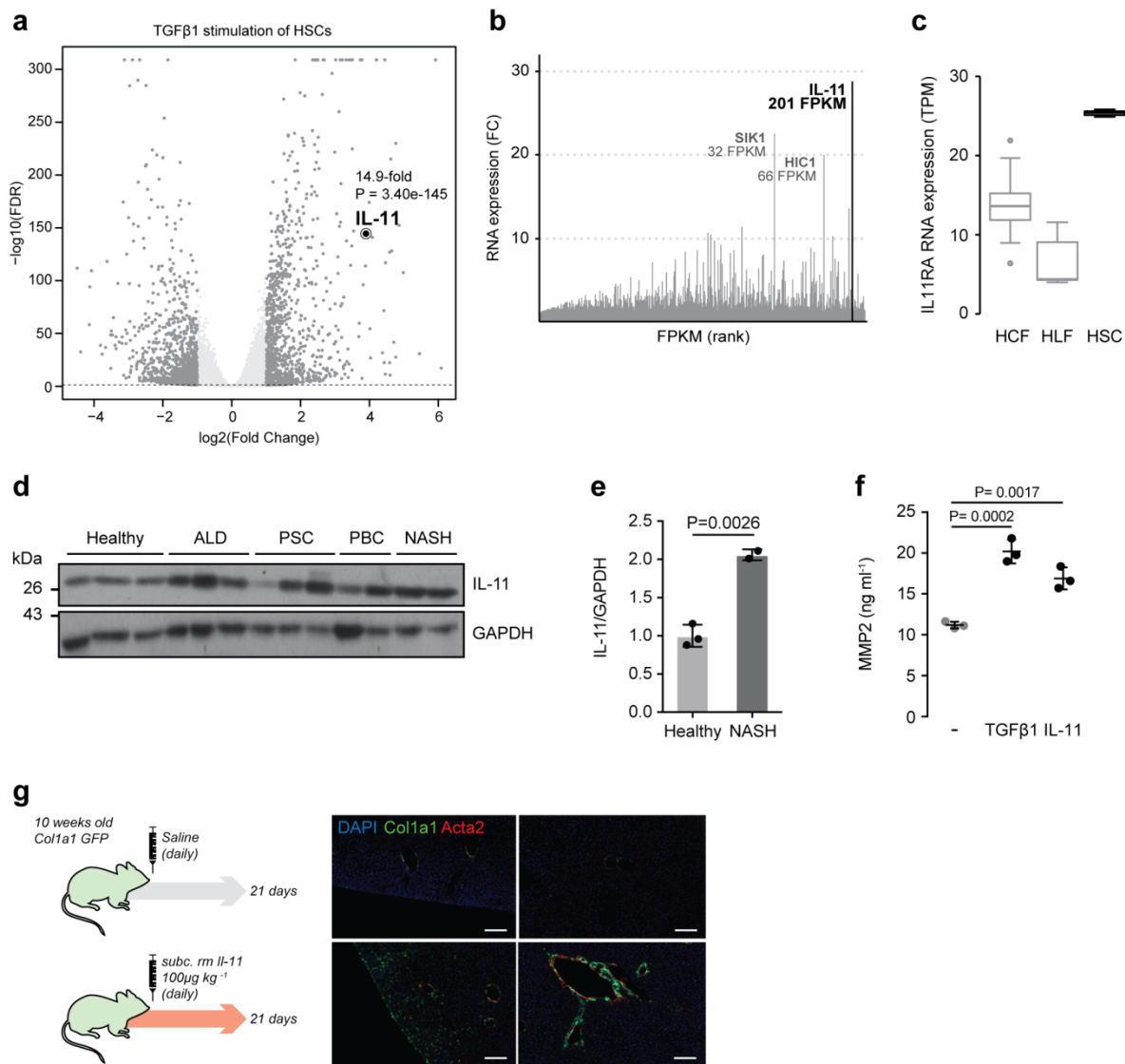
401

### 402 **Competing interests**

403 S.A.C. and S.S. are co-inventors of the patent applications (WO2017103108,  
404 WO2017103108 A2, WO 2018/109174 A2, WO 2018/109170 A2). S.A.C. and S.S.  
405 are co-founders and shareholders of Enleofen Bio PTE LTD, a company (which  
406 S.A.C. is a director of) that develops anti-IL-11 therapeutics. All other authors  
407 declare no competing interest.



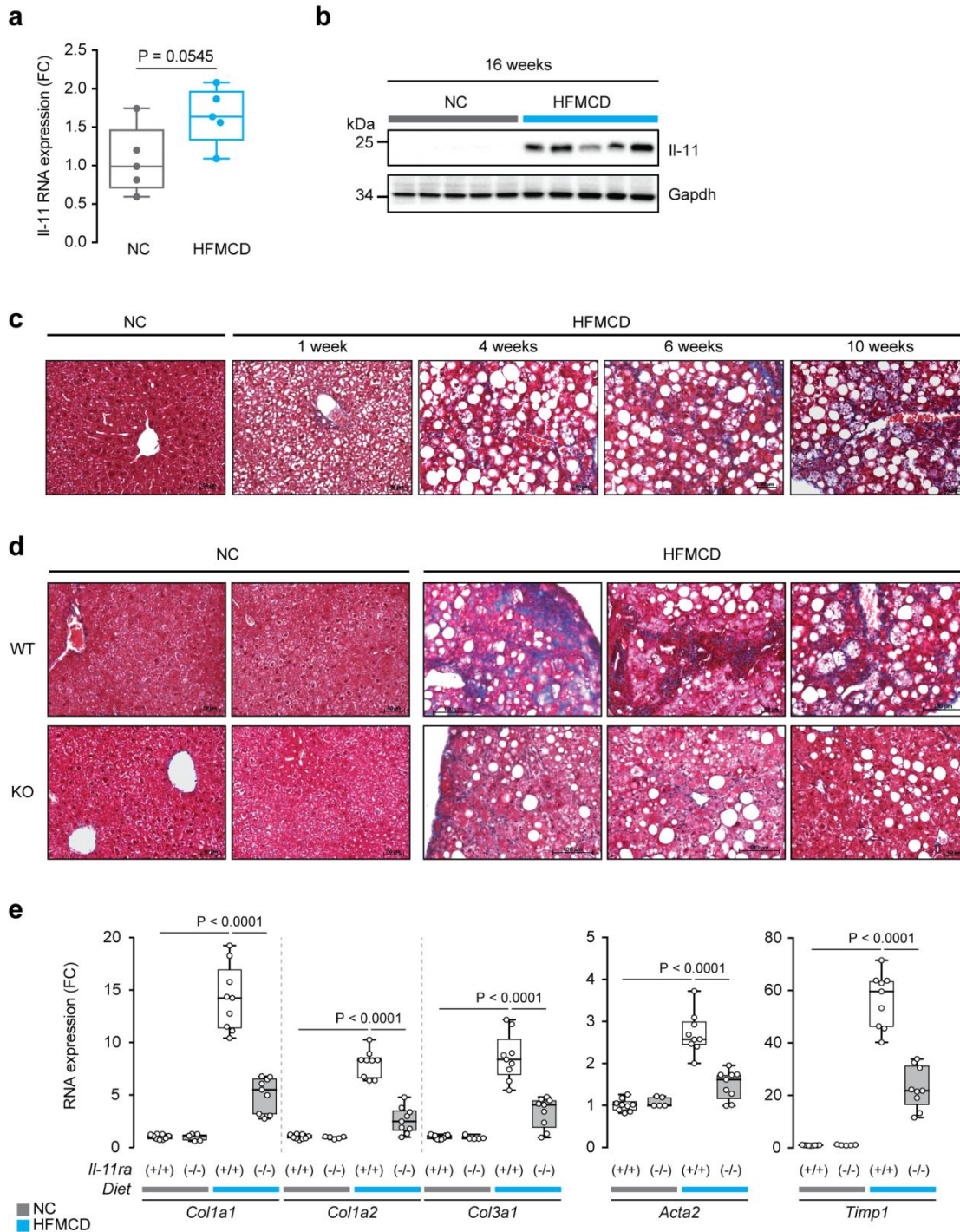
408 **Supplementary Figures**  
409



410  
411

**Supplementary Figure 1. HSCs secrete and respond to IL-11.**

413 **a**, Genome-wide changes in RNA expression in HSCs (n=3) after TGFβ1 stimulation (5 ng ml<sup>-1</sup>, 24 h).  
414 **b**, Stiffness-induced RNA upregulation in humans HSCs (RNA-seq<sup>14</sup>), genes are ranked according to  
415 fragments per kilobase million (FPKM), *IL-11* upregulation is the most highly upregulated gene  
416 genome wide. **c**, IL11RA transcripts in human cardiac fibroblasts (HCF), human lung fibroblasts  
417 (HLF), and human HSC (TPM, Transcript per millions). Data are shown as box-and-whisker with  
418 median (middle line), 25th–75th percentiles (box) and min-max percentiles (whiskers). **d**, Western  
419 blots and **e**, densitometry of IL-11 and GAPDH in human liver samples of healthy individuals and  
420 patients suffering from alcoholic liver disease (ALD), primary sclerosing cholangitis (PSC), primary  
421 biliary cirrhosis (PBC), and non-alcoholic steatohepatitis (NASH). Data are shown as scatter plot with  
422 bar, mean ± s.d; two-tailed Student's *t*-test. **f**, MMP-2 concentration in the supernatant of HSC  
423 (n=3/group) without stimulus (-), with TGFβ1 or IL-11 (5 ng ml<sup>-1</sup>, 24 h) by ELISA. Data are represented  
424 as mean ± s.d; two-tailed Dunnett's test. **g**, Schematic and representative fluorescence images  
425 GFP<sup>+ve</sup> cells of *Col1a1-GFP* mice injected daily with either rml-11 (100 μg kg<sup>-1</sup>) or saline. Sections  
426 were immunostained for Acta2 and counterstained with DAPI (scale bars, 200 μm). FC: fold change.



427

428

429

430 **Supplementary Figure 2. Genetic inhibition of IL-11 signalling reduces hepatic fibrosis.**

431 **a, b**, Effects of 16 weeks of HFMCD diet as compared to NC diet on hepatic (a) *Il-11* mRNA and (b) *Il-*

432 11 protein levels. For (a) and (b) RNA and protein were extracted from the same mice (n=5/group). **c**,

433 Representative Masson's Trichrome images of liver sections from mice fed with NC or HFMCD diet

434 for the indicated treatment duration. **d**, Representative Masson's Trichrome images and **e**, relative

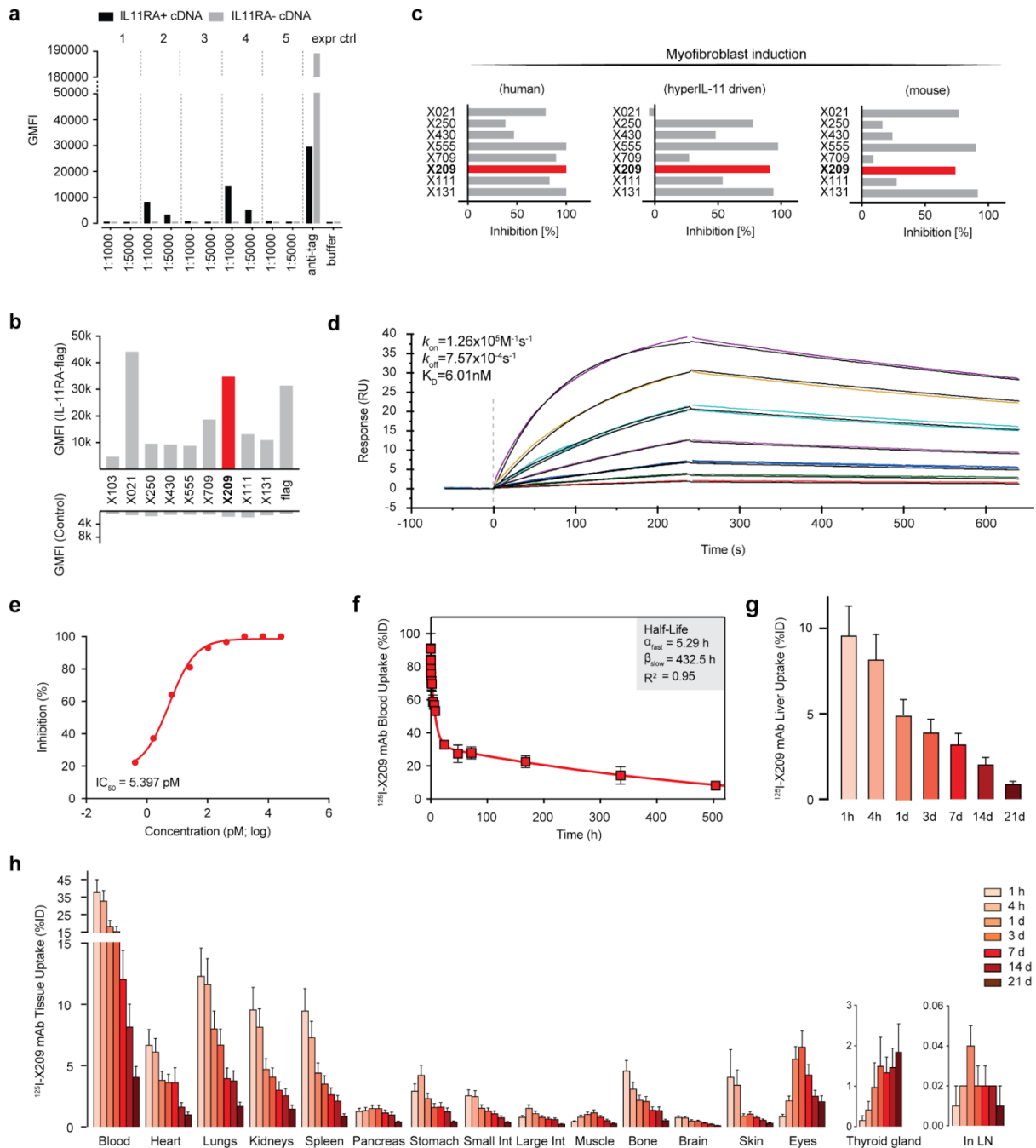
435 RNA expression level of *Acta2*, *Col1a1*, *Col1a2*, and *Col3a1* in livers of *Il11ra*<sup>+/+</sup> (WT) and *Il11ra*<sup>-/-</sup>

436 (KO) mice after 10 weeks of HFMCD diet. **e**, NC WT, n=9; HFMCD WT, n=9; NC KO, n=5; HFMCD

437 KO, n=9. **a, e**, Data are shown as box-and-whisker with median (middle line), 25th–75th percentiles

438 (box) and min-max percentiles (whiskers). **a**, Two-tailed Student's *t*-test; **e**, Sidak-corrected Student's

*t*-test. FC: fold change; NC: normal chow; HFMCD: high fat methionine- and choline-deficient.

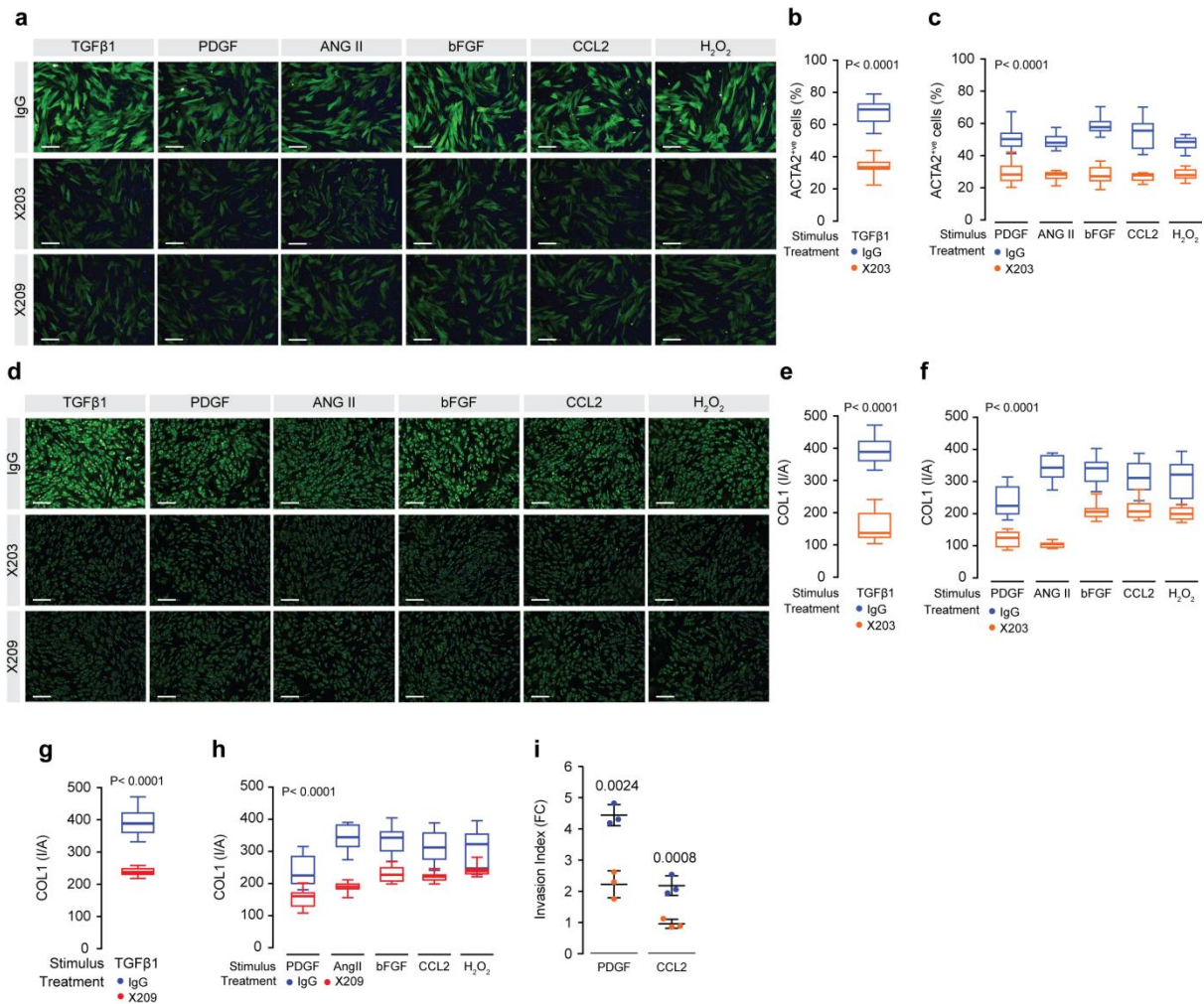


439  
440

441 **Supplementary Figure 3. Development of a neutralizing anti-IL-11RA monoclonal antibody.**

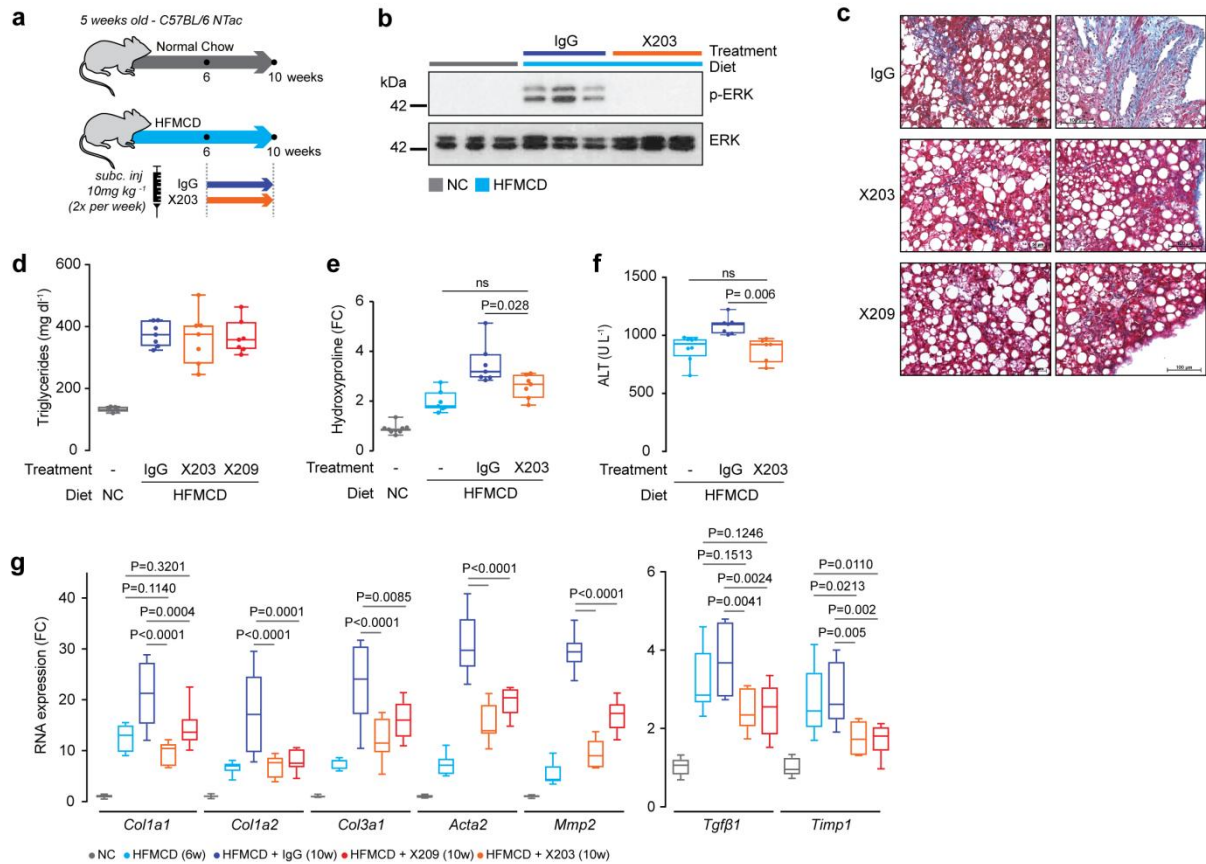
442 **a**, Sera of 5 mice after genetic immunization with human IL11RA. Sera of five animals tested with  
 443 HEK cells transiently transfected with an *IL11RA-flag* or control cDNA vector, incubated with a goat  
 444 anti-mouse fluorescent antibody ( $10 \mu\text{g ml}^{-1}$ ). Cells were then analysed by flow cytometry. Signal is  
 445 geometric mean of the relative fluorescence (GMFI) as measured by flow cytometry. **b**, Supernatants  
 446 of early stage hybridoma cultures on transfected cells. **c**, Inhibition of ACTA2<sup>+</sup> cell transformation of  
 447 TGFβ1-(left), hyperIL-11-(middle) stimulated human atrial fibroblasts and TGFβ1-(right) stimulated  
 448 mouse atrial fibroblasts with purified mouse monoclonal anti-IL11RA candidates ( $6 \mu\text{g ml}^{-1}$ ). **d**, X209  
 449 interactions with IL11RA as determined by SPR (1:1 Langmuir). **e**, Dose-response curve and IC<sub>50</sub>  
 450 value of X209 ( $61 \mu\text{g ml}^{-1}$  to  $4 \mu\text{g ml}^{-1}$ ; 4-fold dilution) in inhibiting MMP2 secretion by HSCs  
 451 stimulated with TGFβ1. **c, e**, TGFβ1 ( $5 \text{ ng ml}^{-1}$ ), Hyper IL-11 ( $0.2 \text{ ng ml}^{-1}$ ); 24 h. **f**, Blood  
 452 pharmacokinetics of <sup>125</sup>I-X209 in mice (n=5). Result was fitted ( $R^2=0.92$ ) to a two-phase exponential  
 453 decay model. **g, h**, Percentage of <sup>125</sup>I-X209 uptake by **(g)** liver (n=5) and **(h)** other organs at the  
 454 indicated time points, following retro-orbital injection. **f-h**, Data are represented as mean + s.d.





455  
456

457 **Supplementary Figure 4. Neutralizing anti-IL-11 and anti-IL11RA antibodies prevent HSC-to-**  
 458 **myfibroblasts transformation.** **a-h**, (**a**, **d**) Representative fluorescence images (scale bars, 200  
 459  $\mu\text{m}$ ) and (**b,c,e-h**) quantification of (**a-c**) ACTA2<sup>+</sup>ve cells and (**d-h**) Collagen 1 immunostaining of HSCs  
 460 treated with (**a,b,d,e,g**) TGFβ1 and other (**a,c,d,f,h**) NASH factors in the presence of IgG control,  
 461 X203, or X209 for 24 h. **i**, Effects of X203 on TGFβ1- and CCL2-induced matrigel invasion of HSCs  
 462 for 48h (n=3). **a-i**, TGFβ1 (5 ng ml<sup>-1</sup>), Hyper IL-11 (0.2 ng ml<sup>-1</sup>), PDGF (20 ng ml<sup>-1</sup>), AngII (100 nM),  
 463 bFGF (10 ng ml<sup>-1</sup>), CCL2 (5 ng ml<sup>-1</sup>), H<sub>2</sub>O<sub>2</sub> (0.2 mM), IgG, X203 and X209 (2  $\mu\text{g ml}^{-1}$ ). **b, c, e-i**, Two-  
 464 tailed Dunnett's test. **b, c, i**, The values of IgG are the same as those shown in **Fig. 2h,j,k**  
 465 respectively. The values of IgG for **g** and **h** are the same as those shown in **c** and **f**, respectively.  
 466 **b, c, e-h**, Data are shown as box-and-whisker with median (middle line), 25th–75th percentiles (box)  
 467 and min-max percentiles (whiskers); **i**, data are represented as mean  $\pm$  s.d. FC: fold change; I/A:  
 468 intensity/area.

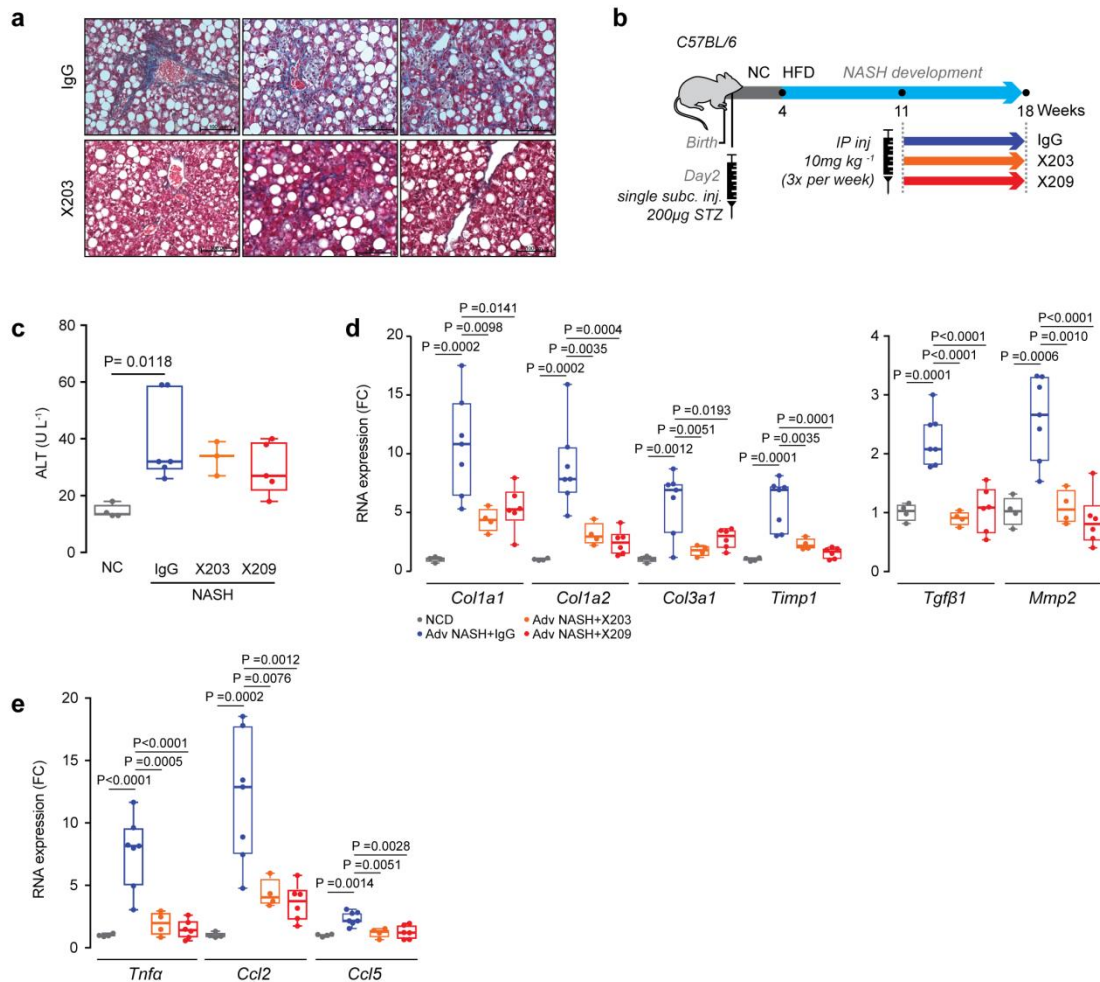


469  
470  
471  
472  
473  
474  
475  
476  
477  
478  
479  
480  
481  
482  
483  
484  
485  
486

**Supplementary Figure 5. Neutralizing anti-IL-11 and anti-IL11RA antibodies inhibit hepatic fibrosis and liver damage.**

**a**, Schematic of therapeutic dosing regimen of X203 in HFMCD fed mice. X203 or IgG (10 mg kg<sup>-1</sup>, twice a week) were administered for 4 weeks, starting from week 6 of the NASH diet. Livers and serum were collected at week 10. **b-g**, Data for therapeutic dosing experiments as shown in **Fig. 3a** and **Supplementary Data Fig. 5a**. **b**, Western blots of liver ERK activation, **c**, representative histological images (Masson's Trichrome staining) of liver sections, **d**, liver triglyceride content, **e**, relative liver hydroxyproline collagen content, and **f**, serum ALT levels from IgG- and X203-treated mice. **d**, NC, n=5; IgG, n=7; X203, n=7, X209, n=7. **e**, The values of NC and HFMCD 6 weeks are the same as those used in **Fig. 2b**; the values of IgG are the same as those used in **Fig. 3c**; X203, n=7. **f**, The values of HFMCD 6 weeks are the same as those used in **Fig. 2c**; the values of IgG are the same as those used in **Fig. 3e**; X203, n=6. **g**, Expression levels of liver pro-fibrotic genes (NC, n=9; HFMCD 6 weeks, n=8; IgG, n=8; X203, n=7; X209, n=9). **d-g**, Data are shown as box-and-whisker with median (middle line), 25th–75th percentiles (box) and min-max percentiles (whiskers); two-tailed, Tukey-corrected Student's *t*-test. FC: fold change; NC: normal chow; HFMCD: high fat methionine- and choline-deficient.

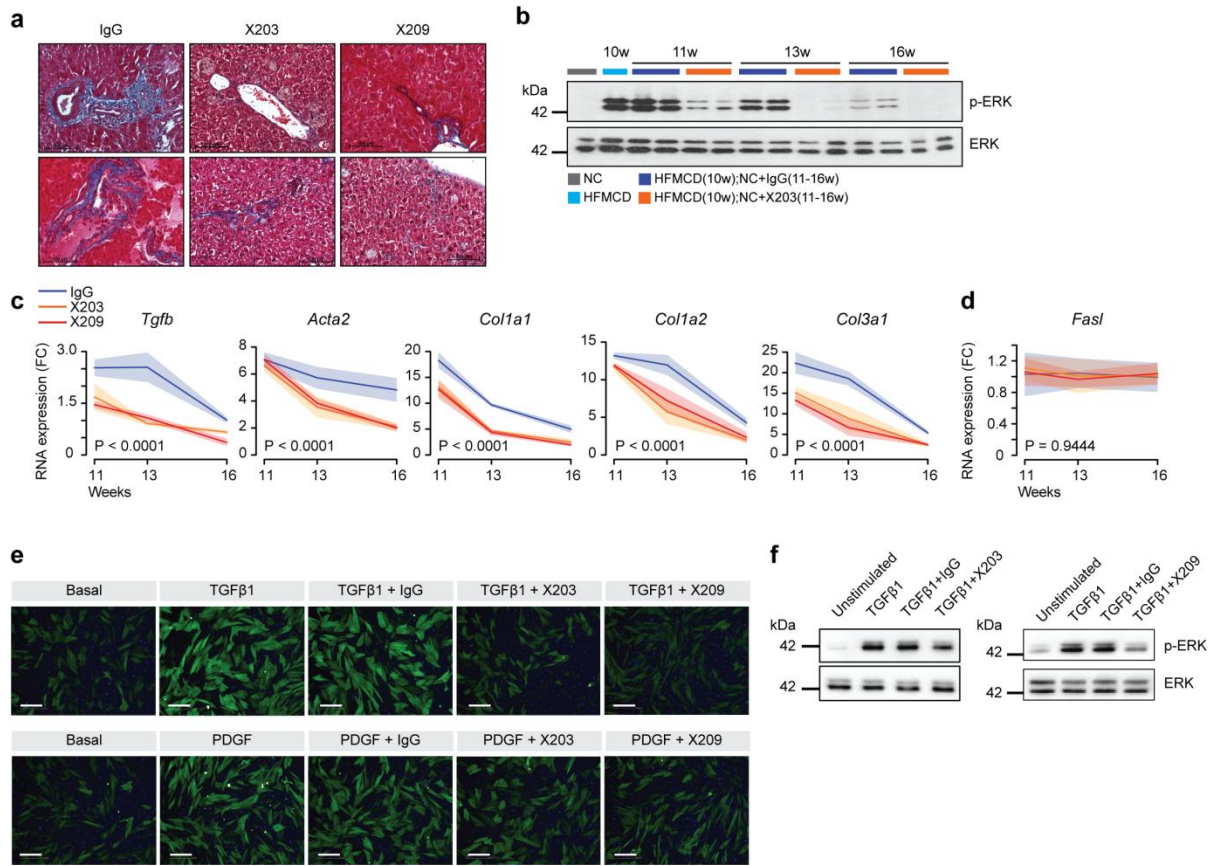




487  
488  
489  
490  
491  
492  
493  
494  
495  
496  
497  
498  
499  
500

**Supplementary Figure 6. Neutralizing anti-IL-11 and anti-IL11RA antibodies reduce hepatic fibrosis and hepatic inflammation in additional NASH models.**

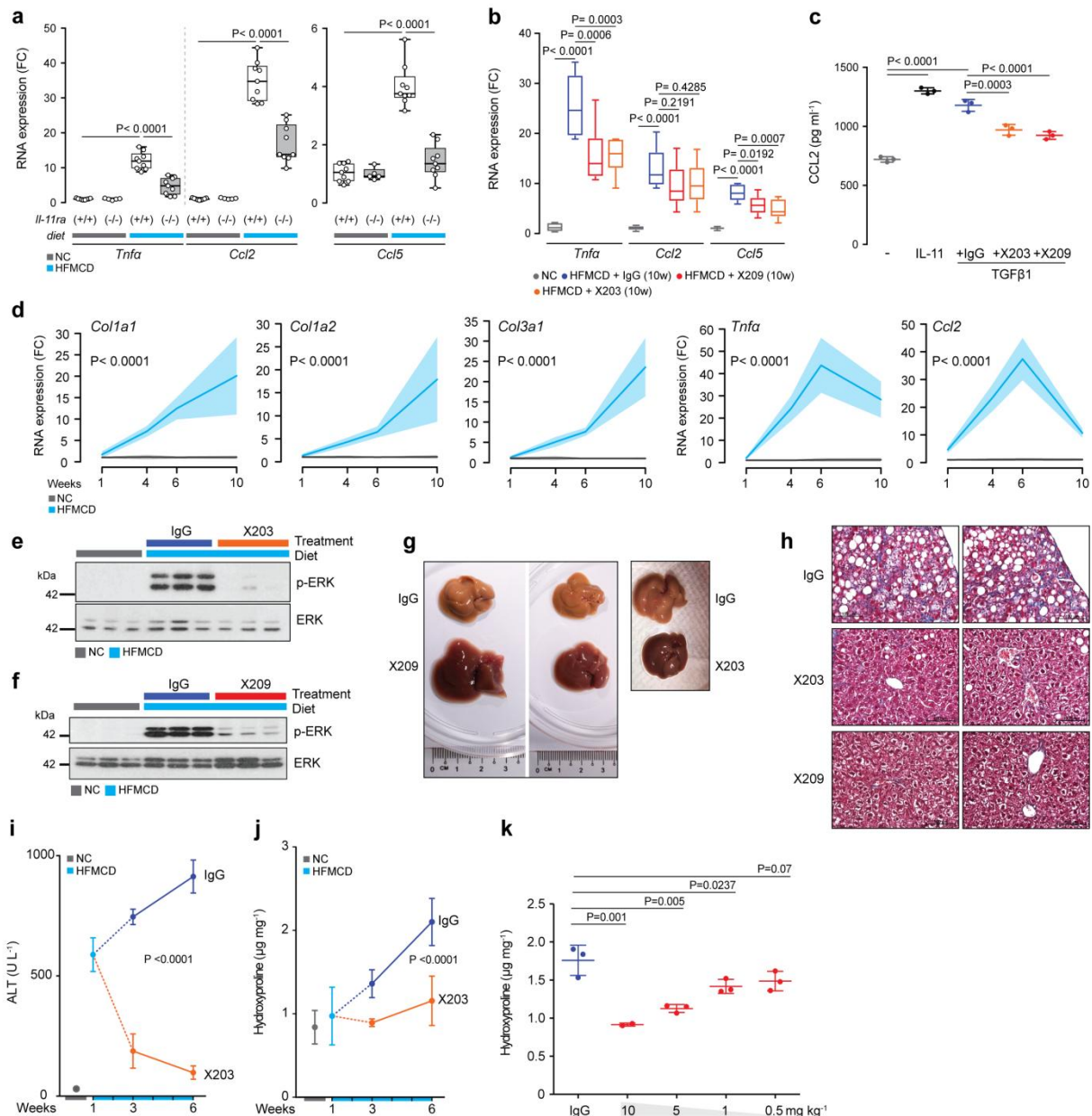
**a**, Representative Masson's Trichrome images of livers from *db/db* mice treated with X203 or IgG. **b**, Schematic representation of the STAM™ model. Mice were injected with 200 µg of Streptozotocin (STZ) 2 days after birth followed by feeding with high fat diet (HFD) at 4-week of age to develop NASH. IgG, X203, and X209 were intraperitoneally injected 3x/week at a dosage of 10 mg kg<sup>-1</sup> for 7 weeks, starting at 11-weeks of age. **c**, Serum ALT levels of STAM™ mice (NC, n=4; IgG, n=6; X203, n=3; X209, n=5). **d, e**, Relative liver mRNA expression levels of fibrosis (**d**) and inflammation (**e**) genes in STAM™ mice treated with X203 or X209 (NC, n=4; IgG, n=7; X203, n=4; X209, n=6). **c-e**, Data are shown as box-and-whisker with median (middle line), 25th–75th percentiles (box) and min-max percentiles (whiskers); two-tailed, Tukey-corrected Student's *t*-test. FC: fold change; NC: normal chow; HFD: high fat diet.



501  
502  
503  
504  
505  
506  
507  
508  
509  
510  
511  
512  
513  
514

**Supplementary Figure 7. Neutralizing anti-IL-11 and anti-IL11RA antibodies reverse hepatic fibrosis.**

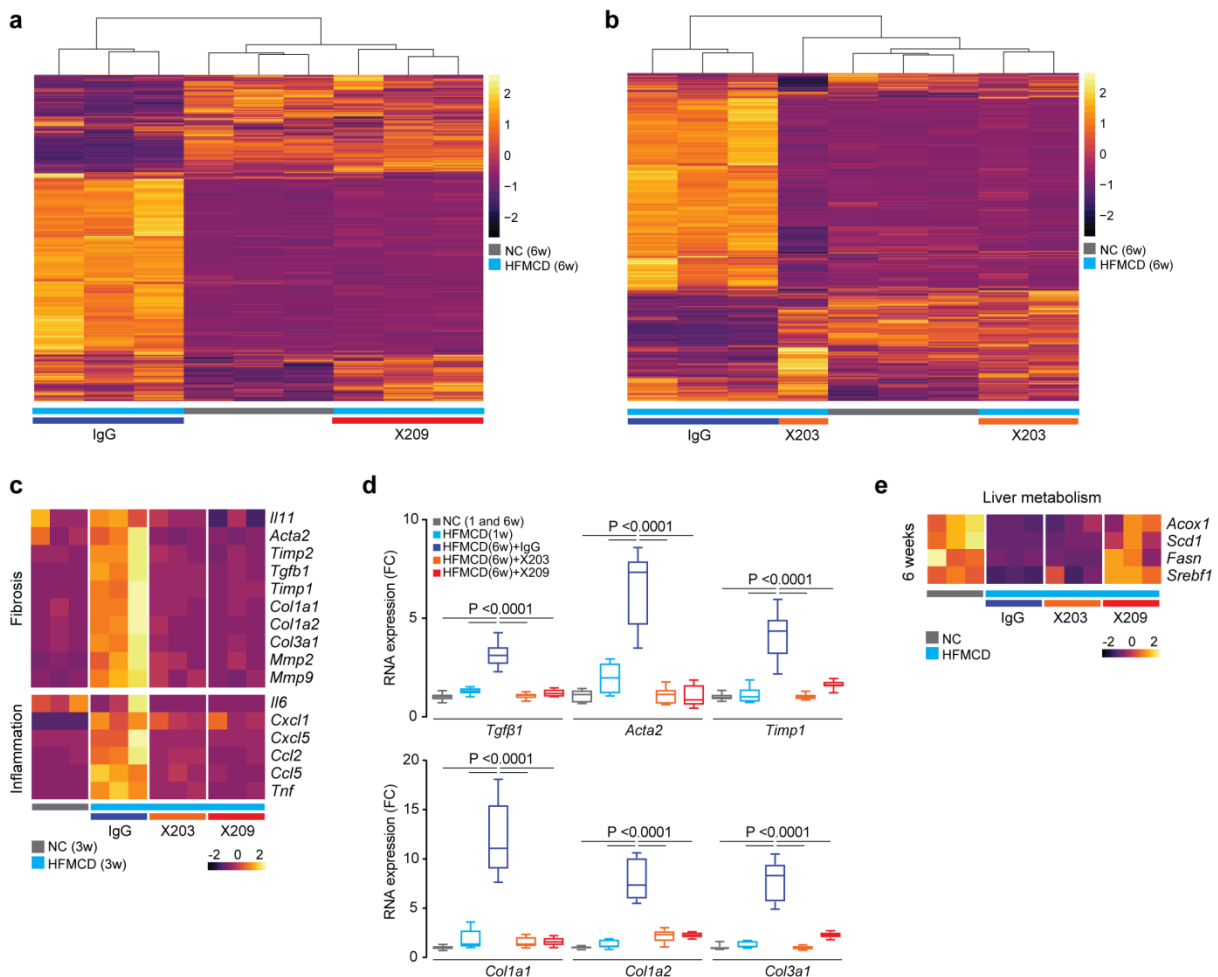
**a**, Representative Masson's Trichrome staining of livers from mice treated with IgG, X203, or X209 for 6 weeks as shown in **Fig. 4a**. **b**, Western blots of hepatic ERK activation status. **c**, **d**, Relative mRNA expression of **(c)** fibrosis markers and **(d)** apoptosis marker (*FasI*) at 1-, 3-, 6- weeks after X203, X209, or IgG treatments ( $n \geq 3$ /group); two-way ANOVA. **e**, **f**, Data from reversal of HSC transformation experiments as shown in **Fig. 4f,g**, TGFβ1 ( $5 \text{ ng ml}^{-1}$ ), PDGF ( $20 \text{ ng ml}^{-1}$ ), IgG, X203, and X209 ( $2 \mu \text{g ml}^{-1}$ ). **e**, Representative fluorescence images (scale bars,  $200 \mu \text{m}$ ) of ACTA2<sup>+ve</sup> immunostaining following incubation with TGFβ1 or with PDGF either prior to or after addition of X203, X209, or IgG. **f**, Western blots of ERK activation status after X203 and X209 treatment in TGFβ1-treated HSC. **c**, **d**, Data are represented as line chart (mean) and transparencies indicate s.d. FC: fold change; NC: normal chow; HFMCD: high fat methionine- and choline-deficient.



515  
516 **Supplementary Figure 8. Neutralizing anti-IL-11 and anti-IL11RA antibodies prevent hepatic**  
517 **fibrosis and reduce hepatic inflammation in HFMCD fed mice.**

518 **a, b**, Relative mRNA expression of inflammation markers (*Tnfa*, *Ccl2*, and *Ccl5*) from the livers of (a)  
519 *Il11ra*<sup>+/+</sup> (WT) and *Il11ra*<sup>-/-</sup> (KO) after 10 weeks of HFMCD diet and (b) mice injected with X203 or  
520 X209 as shown in **Fig. 3a** and **Supplementary Data Fig. 5a**. **a**, NC WT, n=9; HFMCD WT, n=8, NC  
521 KO, n=5; HFMCD KO, n=9. **b**, NC, n=9; IgG, n=8; X203, n=7; X209, n=9. **c**, CCL2 in the supernatants  
522 of HSCs (n=4/group) without stimulus (-), with IL-11, or with TGFβ1 in the presence of IgG, X203, or  
523 X209 by ELISA; IL-11 (5 ng ml<sup>-1</sup>), TGFβ1 (5 ng ml<sup>-1</sup>), IgG, X203, and X209 (2 μg ml<sup>-1</sup>). **d** Relative liver  
524 mRNA expression of fibrosis and inflammation markers from mice fed with NC or HFMCD diets.  
525 Livers were collected at the indicated time points. The values of NC 1 and 6 week(s) for *Tnfa* and  
526 *Ccl2* are the same as those shown in **Fig. 5j**; the values of NC 6 and 10 weeks and HFMCD 6 weeks  
527 are the same as those shown in **Supplementary Data Fig. 5g and 8b** (n≥5/group). **e-k**, Data for  
528 therapeutic dosing experiments as shown in **Fig. 5a**. **e-f**, Western blots of hepatic ERK activation  
529 status after (e) X203 and (f) X209 treatments. **g**, Representative gross liver images, **h**, representative  
530 Masson's Trichrome stained images of livers, **i**, serum ALT levels, **j**, liver hydroxyproline content, and  
531 **k**, dose dependent effects of X209 on total hydroxyproline content in HFMCD-fed mice (n=3/group). **i**,  
532 The values of NC and HFMCD 1 week are the same as those used in **Fig. 2c**, the values of IgG 3 and  
533 6 weeks (2 weeks and 5 weeks treatment, respectively) are the same as those used in **Fig. 5e**. **j**, The  
534 values of NC and HFMCD 1 week diets are the same as those used in **Fig. 2b**, the values of IgG 3

535 and 6 weeks are the same as those used in **Fig. 5g. i,j**, X203 3 weeks, n=5; X203 6 weeks, n=10). **a**,  
 536 **b**, Data are shown as box-and-whisker with median (middle line), 25th–75th percentiles (box) and  
 537 min-max percentiles (whiskers); **c, i-k**, data are represented as mean  $\pm$  s.d.; **d**, data are represented  
 538 as line chart (mean) and transparencies indicate s.d. **a**, Two-tailed, Sidak-corrected Student's *t*-test;  
 539 **b, c**, two-tailed, Tukey-corrected Student's *t*-test; **d, i, j**, two-way ANOVA; **k**, two-tailed Dunnett's test.  
 540 FC: fold change; NC: normal chow; HFMCD: high fat methionine- and choline-deficient.  
 541

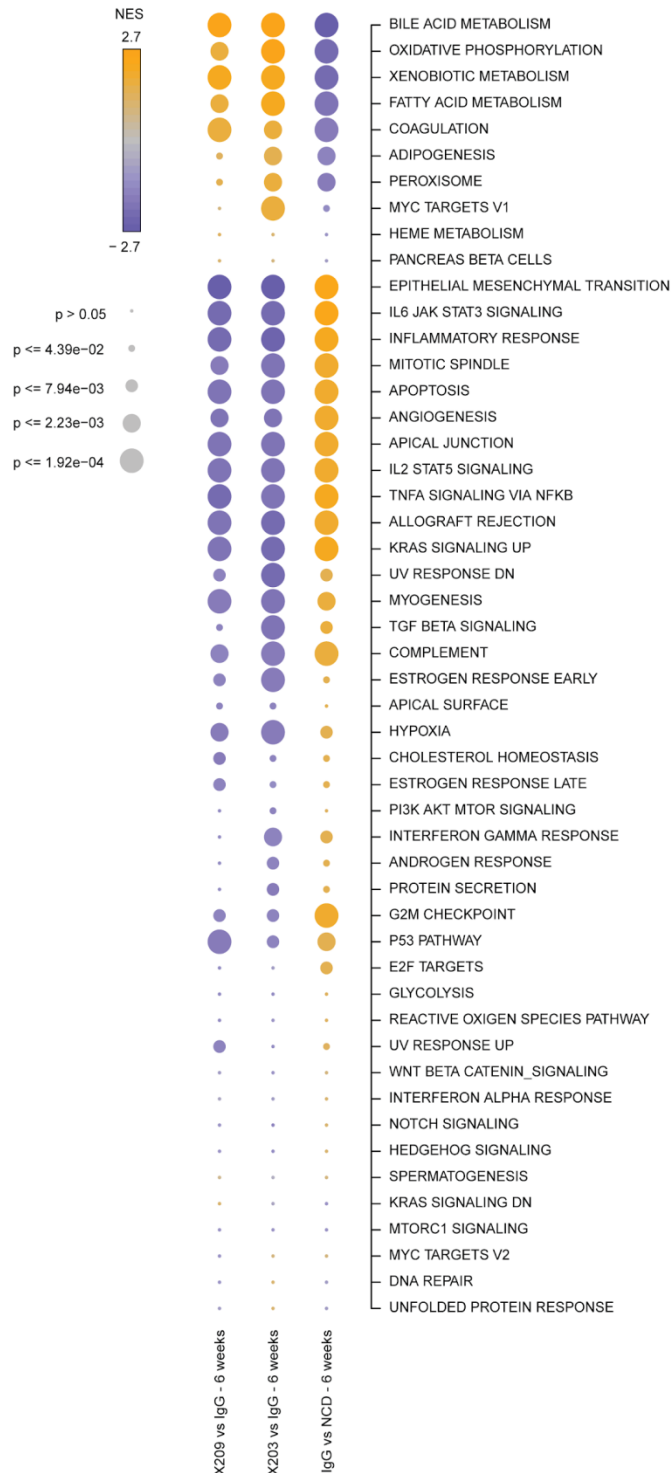


542  
 543

**Supplementary Figure 9. Neutralizing anti-IL-11 or anti-IL11RA antibodies reverse the molecular signature of NASH towards a normal liver profile.**

544 **a-e**, Data for RNA-seq and qPCR confirmation for early therapeutic dosing experiments as shown in  
 545 **Fig 5a. a-b**, Heatmaps showing gene expression levels (Transcripts Per Million mapped reads, TPM)  
 546 across samples for all genes statistically differentially expressed between IgG and (a) X209 or (b)  
 547 X203 treatments. The expression profile for the anti-IL-11 treatments clusters together with the  
 548 profiles in normal chow (NC), suggesting an almost complete reversal of the transcriptional effect of  
 549 HFMCD diet. **c**, Heatmaps showing Z-scores of TPM of pro-fibrotic and pro-inflammatory genes  
 550 indicate that the difference between NC and HFMCD diet were already largely restored by both X203  
 551 and X209 within 2 weeks of starting treatment. **d**, Relative RNA expression levels of fibrosis markers  
 552 after 5 weeks treatment of X203 and X209 by qPCR, which confirms data from RNA-seq. Data are  
 553 shown as box-and-whisker with median (middle line), 25th–75th percentiles (box) and min-max  
 554 percentiles (whiskers); two-tailed, Tukey-corrected Student's *t*-test. The values of NC and HFMCD 1  
 555 week for *Col1a1*, *Col1a2*, and *Col3a1* are the same as those shown in **Supplementary Data Fig. 5g,**  
 556 **8d**; NC, n=9; HFMCD 1 week, n=7, IgG, n=14; X203, n=10; X209, n=8. **e**, Differential expression  
 557 heatmap of lipogenesis and  $\beta$ -oxidation genes showing that X209, more so than X203, improved  
 558 hepatic lipid metabolism as compared to IgG. **a-c, e**, n=3/group. FC: fold change; NC: normal chow;  
 559 HFMCD: high fat methionine- and choline-deficient.  
 560  
 561





562  
563  
564  
565  
566  
567  
568  
569  
570  
571

**Supplementary Figure 10. Gene Set Enrichment Analysis of the effects of anti-IL-11 or anti-IL11RA antibody therapy in mice of HFMC diet as compared to control.**

Bubblemap showing results of the Gene Set Enrichment Analysis (GSEA) for differentially expressed genes found in every comparison after 6-weeks of NC or HFMC diet and antibody therapy, as shown. Each dot represents the Normalized Enrichment Score (NES) for the gene set and its FDR-corrected significance level, summarized by colour and size respectively. Gene sets for the enrichment test were selected from the “H - Hallmark” collection in MSigDB.



572 **References**

- 573 1. Friedman, S. L., Neuschwander-Tetri, B. A., Rinella, M. & Sanyal, A. J.  
574 Mechanisms of NAFLD development and therapeutic strategies. *Nat. Med.*  
575 (2018). doi:10.1038/s41591-018-0104-9
- 576 2. Mederacke, I. *et al.* Fate tracing reveals hepatic stellate cells as dominant  
577 contributors to liver fibrosis independent of its aetiology. *Nat. Commun.* **4**, 2823  
578 (2013).
- 579 3. Friedman, S. L. Hepatic stellate cells: protean, multifunctional, and enigmatic  
580 cells of the liver. *Physiol. Rev.* **88**, 125–172 (2008).
- 581 4. Friedman, S. L. Molecular Regulation of Hepatic Fibrosis, an Integrated Cellular  
582 Response to Tissue Injury. *J. Biol. Chem.* **275**, 2247–2250 (2000).
- 583 5. Higashi, T., Friedman, S. L. & Hoshida, Y. Hepatic stellate cells as key target in  
584 liver fibrosis. *Adv. Drug Deliv. Rev.* **121**, 27–42 (2017).
- 585 6. Hellerbrand, C., Stefanovic, B., Giordano, F., Burchardt, E. R. & Brenner, D. A.  
586 The role of TGF $\beta$ 1 in initiating hepatic stellate cell activation in vivo. *J. Hepatol.*  
587 **30**, 77–87 (1999).
- 588 7. Tsuchida, T. & Friedman, S. L. Mechanisms of hepatic stellate cell activation.  
589 *Nat. Rev. Gastroenterol. Hepatol.* **14**, 397–411 (2017).
- 590 8. Kim, B.-M., Abdelfattah, A. M., Vasan, R., Fuchs, B. C. & Choi, M. Y. Hepatic  
591 stellate cells secrete Ccl5 to induce hepatocyte steatosis. *Sci. Rep.* **8**, 7499  
592 (2018).
- 593 9. Iwaisako, K. *et al.* Origin of myofibroblasts in the fibrotic liver in mice. *Proc. Natl.*  
594 *Acad. Sci. U. S. A.* **111**, E3297–305 (2014).
- 595 10. Schafer, S. *et al.* IL-11 is a crucial determinant of cardiovascular fibrosis. *Nature*  
596 **552**, 110–115 (2017).
- 597 11. Cook, S. *et al.* IL-11 is a therapeutic target in idiopathic pulmonary fibrosis.  
598 (2018). doi:10.1101/336537
- 599 12. Zhu, M. *et al.* IL-11 Attenuates Liver Ischemia/Reperfusion Injury (IRI) through  
600 STAT3 Signaling Pathway in Mice. *PLoS One* **10**, e0126296 (2015).
- 601 13. Yu, J., Feng, Z., Tan, L., Pu, L. & Kong, L. Interleukin-11 protects mouse liver  
602 from warm ischemia/reperfusion (WI/Rp) injury. *Clin. Res. Hepatol.*  
603 *Gastroenterol.* **40**, 562–570 (2016).
- 604 14. Dou, C. *et al.* P300 Acetyltransferase Mediates Stiffness-Induced Activation of

- 605 Hepatic Stellate Cells Into Tumor-Promoting Myofibroblasts. *Gastroenterology*  
606 **154**, 2209–2221.e14 (2018).
- 607 15. Yata, Y. DNase I–hypersensitive sites enhance  $\alpha$ 1(I) collagen gene expression  
608 in hepatic stellate cells. *Hepatology* **37**, 267–276 (2003).
- 609 16. Matsumoto, M. *et al.* An improved mouse model that rapidly develops fibrosis in  
610 non-alcoholic steatohepatitis. *Int. J. Exp. Pathol.* **94**, 93–103 (2013).
- 611 17. Nandurkar, H. H. *et al.* Adult mice with targeted mutation of the interleukin-11  
612 receptor (IL11Ra) display normal hematopoiesis. *Blood* **90**, 2148–2159 (1997).
- 613 18. Lau, J. K. C., Zhang, X. & Yu, J. Animal models of non-alcoholic fatty liver  
614 disease: current perspectives and recent advances. *J. Pathol.* **241**, 36–44  
615 (2017).
- 616 19. Rinella, M. E. *et al.* Mechanisms of hepatic steatosis in mice fed a lipogenic  
617 methionine choline-deficient diet. *J. Lipid Res.* **49**, 1068–1076 (2008).
- 618 20. Wortham, M., He, L., Gyamfi, M., Copple, B. L. & Wan, Y.-J. Y. The Transition  
619 from Fatty Liver to NASH Associates with SAME Depletion in db/db Mice Fed a  
620 Methionine Choline-Deficient Diet. *Dig. Dis. Sci.* **53**, 2761–2774 (2008).
- 621 21. Hemmann, S., Graf, J., Roderfeld, M. & Roeb, E. Expression of MMPs and  
622 TIMPs in liver fibrosis - a systematic review with special emphasis on anti-  
623 fibrotic strategies. *J. Hepatol.* **46**, 955–975 (2007).
- 624 22. Elsharkawy, A. M., Oakley, F. & Mann, D. A. The role and regulation of hepatic  
625 stellate cell apoptosis in reversal of liver fibrosis. *Apoptosis* **10**, 927–939 (2005).
- 626 23. Krizhanovsky, V. *et al.* Senescence of activated stellate cells limits liver fibrosis.  
627 *Cell* **134**, 657–667 (2008).
- 628 24. Schnabl, B., Purbeck, C. A., Choi, Y. H., Hagedorn, C. H. & Brenner, D.  
629 Replicative senescence of activated human hepatic stellate cells is  
630 accompanied by a pronounced inflammatory but less fibrogenic phenotype.  
631 *Hepatology* **37**, 653–664 (2003).
- 632 25. Kisseleva, T. *et al.* Myofibroblasts revert to an inactive phenotype during  
633 regression of liver fibrosis. *Proc. Natl. Acad. Sci. U. S. A.* **109**, 9448–9453  
634 (2012).
- 635 26. Seki, E. *et al.* TLR4 enhances TGF- $\beta$  signaling and hepatic fibrosis. *Nat. Med.*  
636 **13**, 1324–1332 (2007).
- 637 27. Marra, F., Valente, A. J., Pinzani, M. & Abboud, H. E. Cultured human liver fat-  
638 storing cells produce monocyte chemotactic protein-1. Regulation by

- 639 proinflammatory cytokines. *J. Clin. Invest.* **92**, 1674–1680 (1993).
- 640 28. Koyama, Y. & Brenner, D. A. Liver inflammation and fibrosis. *J. Clin. Invest.* **127**,  
641 55–64 (2017).
- 642 29. Makarev, E. *et al.* Common pathway signature in lung and liver fibrosis. *Cell*  
643 *Cycle* **15**, 1667–1673 (2016).
- 644 30. Ma, J., Song, X., Xu, X. & Mou, Y. Cancer-Associated-Fibroblasts Promote the  
645 Chemo-Resistance in Gastric Cancer through Secreting IL-11 targeting  
646 JAK/STAT3/Bcl2 Pathway. *Cancer Res. Treat.* (2018). doi:10.4143/crt.2018.031
- 647 31. Marusyk, A. *et al.* Non-cell-autonomous driving of tumour growth supports sub-  
648 clonal heterogeneity. *Nature* **514**, 54–58 (2014).
- 649 32. Arijs, I. *et al.* Mucosal gene signatures to predict response to infliximab in  
650 patients with ulcerative colitis. *Gut* **58**, 1612–1619 (2009).
- 651 33. Elshabrawy, H. A. *et al.* IL-11 facilitates a novel connection between RA joint  
652 fibroblasts and endothelial cells. *Angiogenesis* (2018). doi:10.1007/s10456-017-  
653 9589-y
- 654 34. Brischoux-Boucher, E. *et al.* IL11RA-related Couzon-like autosomal recessive  
655 craniosynostosis in ten new patients: resemblances and differences. *Clin.*  
656 *Genet.* (2018). doi:10.1111/cge.13409.

## 657 **Material and Methods**

658

### 659 **Animal experiments**

660 All animal procedures were approved and conducted in accordance with the  
661 SingHealth Institutional Animal Care and Use Committee (IACUC). All mice were  
662 provided food and water *ad libitum*.

663

#### 664 *Mouse models of NASH*

##### 665 *High fat methionine- and choline-deficient (HFMCD) diet fed mice*

666 Five-week old male C57BL/6N mice were fed methionine- and choline-deficient diet  
667 supplemented with 60 kcal% fat (A06071301B, Research Diets); control mice were  
668 fed with normal chow (NC, Specialty Feeds). Durations of diet and antibody  
669 therapies varied as outlined in the main text.

670

##### 671 *MCD diet fed Leprdb/db mice*

672 Male BKS.Cg-Dock7m+/+LeprdbJ (*db/db*) mice were used when they are at 12-  
673 weeks of age and at the hepatic steatosis stage. Animals were then fed methionine-  
674 and choline-deficient diet (MCD, A02082002BRi, Research Diets) for 8 weeks;  
675 control mice were of the same genotype. Durations of diet and antibody therapies  
676 varied as outlined in the main text.

677

##### 678 *Model of streptozotocin-induced diabetes and advanced NASH*

679 We engaged contract research organization (CRO) service from SMC Laboratories,  
680 Japan to perform this study. Briefly, two-day old male wild-type mice received a  
681 single subcutaneous injection of 200 µg streptozotocin (STZ, S1030, Sigma),  
682 followed by feeding with high fat diet (HFD32, CLEA Japan) from when they were of  
683 4-weeks of age until the end of the experiment at 18-weeks. Control mice received  
684 NC diet for the duration of the experiment. Mice received either IgG, X203 or X209  
685 from week 11 until the end of the experiment.

686

##### 687 *Il11ra-deleted mice*

688 Mice lacking functional alleles for *Il11ra* (*Il11ra*<sup>-/-</sup>) were on C57Bl/6J genetic  
689 background (B6.129S1-*Il11ra*<sup>tm1Wehi</sup>/J, Jackson's Laboratory). Both *Il11ra*<sup>-/-</sup> mice and  
690 their wild-type littermates (*Il11ra*<sup>+/+</sup>) were fed with HFMCD for 10 weeks from 5-  
691 weeks of age to develop NASH; control mice were fed with NC for the same  
692 duration.

693

##### 694 ***In vivo* administration of Il-11**

695 Recombinant mouse Il-11 (rmil-11) was reconstituted to a concentration of 50 µg ml<sup>-1</sup>  
696 in saline. Ten-week-old male *Col1a1-GFP* reporter mice<sup>1</sup> and wild-type C57BL/6J  
697 mice received daily subcutaneous injection of either 100 µg kg<sup>-1</sup> of rmil-11 or  
698 identical volume of saline for 21 days.

699

##### 700 ***In vivo* administration of anti-IL-11 or anti-IL11RA monoclonal antibodies**

701 Mice were injected intraperitoneally with either anti-IL-11 (X203) or anti-IL11RA  
702 (X209) or an identical amount of IgG isotype control for the treatment durations  
703 outlined in the main text.

704

##### 705 **Antibodies**

706 ACTA2 (ab7817, Abcam), CD45 (103102, Biolegend), Collagen I (ab34710, Abcam),

707 p-ERK1/2 (4370, Cell Signaling), ERK1/2 (4695, Cell Signaling), GAPDH (2118, Cell  
708 Signaling), IgG (Aldevron), IL-11 (X203, Aldevron), IL11RA (X209, Aldevron), Ly6C  
709 (128039, Biolegend), TGF $\beta$ 1 (141402, Biolegend), anti rabbit HRP (7074, CST), anti  
710 mouse HRP (7076, CST).

711

### 712 **Recombinant proteins**

713 Commercial recombinant proteins: Human angiotensin II (A9525, Sigma-Aldrich),  
714 human CCL2 (279-MC-050/CF, R&D Systems), human bFGF (233-FB-025, R&D  
715 Systems), human IL-11 (PHC0115, Life Technologies), human PDGF (220-BB-010,  
716 R&D Systems), human TGF $\beta$ 1 (PHP143B, Bio-Rad), and mouse TGF $\beta$ 1 (7666-MB-  
717 005, R&D Systems).

718 Custom recombinant proteins: Mouse IL-11 (UniProtKB: P47873) were synthesized  
719 without the signal peptide, HyperIL-11 was constructed using a fragment of IL11RA  
720 (amino acid residues 1–317; UniProtKB: Q14626) and IL-11 (amino acid residues  
721 22–199, UniProtKB: P20809) as described previously<sup>3</sup>. All custom recombinant  
722 proteins were synthesized by GenScript using a mammalian expression system.

723

### 724 **Chemical**

725 Hydrogen Peroxide (H<sub>2</sub>O<sub>2</sub>, 31642, Sigma)

726

### 727 **Cell culture**

728 Cells (HSCs or fibroblasts) were grown and maintained at 37°C and 5% CO<sub>2</sub>. The  
729 growth medium was renewed every 2–3 days and cells were passaged at 90%  
730 confluence using standard trypsinization techniques. All the experiments were  
731 carried out at low cell passage (<P4) and cells were serum-starved for 16 h prior to  
732 respective stimulations. Stimulated cells were compared to unstimulated cells that  
733 have been grown for the same duration under the same conditions (serum-free  
734 media), but without the stimuli.

735

#### 736 *Primary human atrial fibroblasts*

737 Human atrial fibroblasts were prepared and cultured as described previously<sup>2</sup>.

738

#### 739 *Primary human hepatic stellate cells (HSCs)*

740 HSCs (5300, ScienCell) were cultured in stellate cells complete media (5301,  
741 ScienCell) on poly-L-lysine-coated culture plates (2  $\mu$ g cm<sup>-2</sup>, 0403, ScienCell).

742

### 743 **Operetta high throughput phenotyping assay**

744 The Operetta phenotyping assay was performed mostly as described previously<sup>3</sup>  
745 with minor modifications described here: HSCs were seeded in 96-well black  
746 CellCarrier plates (PerkinElmer) at a density of 5x10<sup>3</sup> cells per well. Following  
747 experimental conditions, cells were fixed in 4% paraformaldehyde (PFA, 28908,  
748 Thermo Fisher Scientific), permeabilized with 0.1% Triton X-100 (Sigma) and non-  
749 specific sites were blocked with 0.5% BSA and 0.1% Tween -20 in PBS. Cells were  
750 incubated overnight (4°C) with primary antibodies (1:500), followed by incubation  
751 with the appropriate AlexaFluor 488 secondary antibodies (1:1000). EdU-Alexa Fluor  
752 488 was incorporated using a Click-iT EdU Labelling kit (C10350, Thermo Fisher  
753 Scientific) according to manufacturer's protocol. Cells were counterstained with 1  $\mu$ g  
754 ml<sup>-1</sup> DAPI (D1306, Thermo Fisher Scientific) in blocking solution. Each condition was  
755 imaged from duplicated wells and a minimum of 7 fields per well using Operetta  
756 high-content imaging system 1483 (PerkinElmer). The quantification of ACTA2<sup>+ve</sup>



757 cells was measured using Harmony v3.5.2 (PerkinElmer). The measurement of  
758 fluorescence intensity per area of Collagen I (normalized to the number of cells) was  
759 performed with Columbus 2.7.1 (PerkinElmer).

760

### 761 **Matrigel invasion assay**

762 The invasive behavior of human HSCs was assayed using 24-well Boyden chamber  
763 invasion assays (Cell Biolabs Inc.). Equal numbers of HSCs in serum-free HSC  
764 media were seeded in triplicates onto the ECM-coated matrigel and were allowed to  
765 invade towards HSC media containing 0.2% FBS. After 48 h of incubation with  
766 stimuli, media was aspirated and non-invasive cells were removed using cotton  
767 swabs. The cells that invaded towards the bottom chamber were stained with cell  
768 staining solution (Cell Biolabs Inc.) and invasive cells from 5 non-overlapping fields  
769 of each membrane were imaged and counted under 40x magnification. For antibody  
770 inhibition experiments, HSCs were pretreated with X203, X209, or IgG control  
771 antibodies for 15 m prior to addition of stimuli.

772

### 773 **Generation of mouse monoclonal antibodies against IL11RA**

#### 774 *Genetic immunisation and screening for specific binding*

775 A cDNA encoding amino acids 23-422 of human IL11RA was cloned into expression  
776 plasmids (Aldevron). Mice were immunised by intradermal application of DNA-coated  
777 gold-particles using a hand-held device for particle-bombardment. Cell surface  
778 expression on transiently transfected HEK cells was confirmed with anti-tag  
779 antibodies recognising a tag added to the N-terminus of the IL11RA protein. Sera  
780 were collected after 24 days and a series of immunisations and tested in flow  
781 cytometry on HEK293 cells transiently transfected with the aforementioned  
782 expression plasmids. The secondary antibody was goat anti-mouse IgG R-  
783 phycoerythrin-conjugated antibody (Southern Biotech, #1030-09) at a final  
784 concentration of  $10 \mu\text{g ml}^{-1}$ . Sera were diluted in PBS containing 3% FBS. Interaction  
785 of the serum was compared to HEK293 cells transfected with an irrelevant cDNA.  
786 Specific reactivity was confirmed in 2 animals and antibody-producing cells were  
787 isolated from these animals and fused with mouse myeloma cells (Ag8) according to  
788 standard procedures. Supernatant of hybridoma cultures were incubated with HEK  
789 cells expressing an IL11RA-flag construct and hybridomas producing antibodies  
790 specific for IL11RA were identified by flow cytometry.

791

#### 792 *Identification of neutralizing anti-IL11RA antibodies*

793 Antibodies that bound to IL11RA-flag cells but not to the negative control were  
794 considered specific binders and subsequently tested for anti-fibrotic activity on  
795 human and mice atrial fibroblasts as described by Schafer et al<sup>2</sup>. Briefly, primary  
796 human or mouse fibroblasts were stimulated with human or mouse TGF $\beta$ 1,  
797 respectively ( $5 \text{ ng ml}^{-1}$ ; 24 h) in the presence of the antibody candidates ( $6 \mu\text{g ml}^{-1}$ ).  
798 TGF $\beta$ 1 stimulation results in an upregulation of endogenous IL-11, which if  
799 neutralized, blocks the pro-fibrotic effect of TGF $\beta$ 1. The fraction of activated  
800 myofibroblasts (ACTA2<sup>+ve</sup> cells) was measured on the Operetta platform as  
801 described above to estimate the neutralization potential of the antibody candidates.  
802 In order to block potential trans-signalling effects, antibodies were also screened in  
803 the context of hyperIL-11 stimulation of human fibroblasts ( $200 \text{ pg ml}^{-1}$ ). We detected  
804 three specific and neutralizing IL11RA antibodies, of which X209 was taken forward  
805 for *in vivo* studies. The same procedures were performed to obtain a neutralizing  
806 antibody that binds to the ligand IL-11, as detailed by Cook et al<sup>3</sup>.

807

### 808 *Binding kinetics of X209 to IL11RA*

809 Binding of X209 to human IL11RA was measured on Biacore T200 (GE Healthcare).  
810 X209 was immobilized onto an anti-mouse capture chip. Interaction assays were  
811 performed with HEPES-buffered saline pH 7.4 containing 0.005% P20 and 0.5%  
812 BSA. A concentration range (1.56 nM to 100 nM) of the analyte (human IL11RA) was  
813 injected over X209 and reference surfaces at a flow rate of 40  $\mu\text{l min}^{-1}$ . Binding to  
814 mouse IL11ra1 was confirmed on Octet system (ForteBio) using a similar strategy. All  
815 sensograms were aligned and double-referenced<sup>5</sup>. Affinity and kinetic constants  
816 were determined by fitting the corrected sensograms with 1:1 Langmuir model. The  
817 equilibrium binding constant  $K_D$  was determined by the ratio of  $k_d/k_a$ .

818

### 819 *X209 IC<sub>50</sub> measurement.*

820 HSCs were stimulated with TGF $\beta$ 1 (5 ng ml<sup>-1</sup>, 24 h) in the presence of IgG (4  $\mu\text{g ml}^{-1}$ )  
821 and varying concentrations of X209 (4  $\mu\text{g ml}^{-1}$  to 61 pg ml<sup>-1</sup>; 4-fold dilutions).  
822 Supernatants were collected and assayed for the amount of secreted MMP2. Dose-  
823 response curves were generated by plotting the logarithm of X209 tested  
824 concentration (pM) versus corresponding percent inhibition values using least  
825 squares (ordinary) fit. The IC<sub>50</sub> value was calculated using log(inhibitor) versus  
826 normalized response-variable slope equation.

827

### 828 *Blood pharmacokinetics and biodistribution*

829 C57BL/6J mice (10-12-weeks old) were retro-orbitally injected (left eye) with 100  $\mu\text{l}$   
830 of freshly radiolabeled <sup>125</sup>I-X209 (5 $\mu\text{Ci}$ , 2.5  $\mu\text{g}$ ) in PBS. Mice were anesthetized with  
831 2% isoflurane and blood were collected at several time points (2, 5, 10, 15, 30 m, 1,  
832 2, 4, 6, 8 h, 1, 2, 3, 7, 14 and 21 days) post injection via submandibular bleeding. For  
833 biodistribution studies, blood was collected via cardiac puncture and tissues were  
834 harvested at the following time points: 1, 4 h, 1, 3, 7, 14, 21 days post injection. The  
835 radioactivity contents were measured using a gamma counter (2480 Wizard2, Perkin  
836 Elmer) with decay-corrections (100x dilution of 100  $\mu\text{l}$  dose). The measured  
837 radioactivity was normalized to % injected dose/g tissue.

838

### 839 **Precision cut liver slices (PCLS) and Western blotting of NASH patient liver**

840 We engaged CRO service (FibroFind, UK) to perform these studies. Briefly, human  
841 PCLS were cut and incubated with TGF $\beta$ 1 for 24 h. ELISA from the supernatant was  
842 performed using Human IL-11 DuoSet (DY218, R&D Systems). This CRO also  
843 collected liver biopsies from patients undergoing liver resections for cancers where  
844 adjacent, non-cancerous tissue was collected for molecular studies. Patients had  
845 either no documented intrinsic liver disease (controls) or previously documented  
846 alcoholic liver disease, primary biliary cirrhosis, primary sclerosing cholangitis or  
847 NASH. For confidentiality reasons no further information was provided for these  
848 samples.

849

### 850 **RNA-seq**

#### 851 *Generation of RNA-seq libraries*

852 Total RNA was quantified using Qubit RNA high sensitivity assay kit (Thermo Fisher  
853 Scientific) and RNA integrity number (RIN) was assessed using the LabChip GX  
854 RNA Assay Reagent Kit (Perkin Elmer). TruSeq Stranded mRNA Library Preparation  
855 Kit (Illumina) was used to prepare the transcript library according to the  
856 manufacturer's protocol. All final libraries were quantified using KAPA library

857 quantification kits (KAPA Biosystems). The quality and average fragment size of the  
858 final libraries were determined using LabChip GX DNA High Sensitivity Reagent Kit  
859 (Perkin Elmer). Libraries were pooled and sequenced on a NextSeq 500 benchtop  
860 sequencer (Illumina) using NextSeq 500 High Output v2 kit and paired-end 75-bp  
861 sequencing chemistry.

862

### 863 *RNA-seq analysis*

864 *Stiffness-induced RNA regulation in hepatic stellate cells*: Normalized gene  
865 expression values were downloaded from Dou et al<sup>5</sup>. Lowly expressed genes (FPKM  
866 at baseline  $\geq 2$ ) were removed from the analysis and fold changes were calculated  
867 as average FPKM in HSCs on stiff surface divided by average FPKM in HSCs on  
868 soft surface. The fold change of RNA expression for upregulated genes (f.c.  $>1$ ) was  
869 plotted and genes were ranked according to their average FPKM value.

870 *TGFB1 stimulation of human hepatic stellate cells and antibody treatment in*

871 *HFMCD*: Sequenced libraries were demultiplexed using bcl2fastq v2.19.0.316 with  
872 the `--no-lane-splitting` option. Adapter sequences were then trimmed using

873 trimmomatic<sup>6</sup> v0.36 in paired end mode with the options `MAXINFO:35:0.5`

874 `MINLEN:35`. Trimmed reads were aligned to the *Homo sapiens* GRCh38 using

875 STAR<sup>7</sup> v. 2.2.1 with the options `--outFilterType BySJout --outFilterMultimapNmax 20`

876 `--alignSJoverhangMin 8 --alignSJDBoverhangMin 1 --outFilterMismatchNmax 999 --`

877 `alignIntronMin 20 --alignIntronMax 1000000 --alignMatesGapMax 1000000` in paired

878 end, single pass mode. Only unique alignments were retained for counting. Counts

879 were calculated at the gene level using the FeatureCounts module from subread<sup>8</sup> v.

880 1.5.1, with the options `-O -s 2 -J -T 8 -p -R -G`. The Ensembl release 92 hg38 GTF

881 was used as annotation to prepare STAR indexes and for FeatureCounts.

882 For the antibody treatment experiments in mouse, libraries were treated as for the

883 human samples, only using mm10 Ensembl release 86 genome and annotation.

884 Differential expression analyses were performed in R 3.4.1 using the Bioconductor

885 package DESeq2<sup>9</sup> 1.18.1, using the Wald test for comparisons and including the

886 variance shrinkage step setting a significance threshold of 0.05.

887 Gene set enrichment analyses (GSEA) were performed in R 3.4.1 using the fgsea

888 package and the MSigDB Hallmark genesets<sup>10,11</sup>, performing 100000 iterations. The

889 “stat” column of the DESeq2 results output was used as ranked input for each

890 enrichment, taking only mouse genes with one-to-one human orthologs.

891

### 892 **Mass cytometry by Time of Flight (CyTOF)**

893 Immune cells were isolated from liver as described previously<sup>12</sup>. Liver tissues were

894 minced and digested with 100  $\mu\text{g ml}^{-1}$  Collagenase IV and 20 U  $\text{ml}^{-1}$  DNase I, at 37°C

895 for 1 h. Following digestion, cells were passed through strainer to obtain single cell

896 suspension and subjected to percoll gradient centrifugation for isolation of immune

897 cells. CyTOF staining was performed as previously described<sup>13</sup>. Cells were thawed

898 and stained with cisplatin (Fluidigm) to identify live cells, followed by staining with

899 metal-conjugated CD45 antibody, for barcoding purpose. After barcoding, cells were

900 stained with metal-conjugated cell surface antibody (Ly6C). Cells were then fixed

901 with 1.6% PFA, permeabilized with 100% methanol, and subjected to intracellular

902 antibody staining (TGF $\beta$ 1). Cells were finally labeled with DNA intercalator before

903 acquisition on Helios mass cytometer (Fluidigm). For analysis, first live single cells

904 were identified, followed by debarcoding to identify individual samples. Manual

905 gating was performed using Flowjo software (Flowjo, LLC, USA).

906

## 907 **Enzyme-linked immunosorbent assay (ELISA) and colorimetric assays**

908 The levels of IL-11 and MMP-2 in equal volumes of cell culture media were  
909 quantified using Human IL-11 Quantikine ELISA kit (D1100, R&D Systems) and  
910 Total MMP-2 Quantikine ELISA kit (MMP200, R&D Systems), respectively. Mouse  
911 serum levels of alanine aminotransferase (ALT) was measured using Alanine  
912 Transaminase Activity Assay Kit (ab105134, abcam). Total secreted collagen in the  
913 cell culture supernatant was quantified using Sirius red collagen detection kit (9062,  
914 Chondrex). Total hydroxyproline content in the livers was measured using  
915 Quickzyme Total Collagen assay kit (Quickzyme Biosciences). Liver Triglycerides  
916 (TG) measurements were performed using triglyceride colorimetric assay kit  
917 (10010303, Cayman). All ELISA and colorimetric assays were performed according  
918 to the manufacturer's protocol.

919

## 920 **Quantitative polymerase chain reaction (qPCR)**

921 Total RNA was extracted from either the snap-frozen liver tissues or HSCs lysate  
922 using Trizol (Invitrogen) followed by RNeasy column (Qiagen) purification. The  
923 cDNAs were synthesized with iScript<sup>TM</sup> cDNA synthesis kit (Bio-Rad) according to  
924 manufacturer's instructions. Gene expression analysis was performed on duplicate  
925 samples with either TaqMan (Applied Biosystems) or fast SYBR green (Qiagen)  
926 technology using StepOnePlus<sup>TM</sup> (Applied Biosystem) over 40 cycles. Expression  
927 data were normalized to *GAPDH* mRNA expression and fold change was calculated  
928 using  $2^{-\Delta\Delta C_t}$  method. The sequences of specific TaqMan probes and SYBR green  
929 primers are available upon request.

930

## 931 **Immunoblotting**

932 Western blots were carried out on total protein extracts from HSCs and liver tissues.  
933 Both cells and frozen tissues were homogenized in radioimmunoprecipitation assay  
934 (RIPA) buffer containing protease and phosphatase inhibitors (Thermo Scientific),  
935 followed by centrifugation to clear the lysate. Protein concentrations were  
936 determined by Bradford assay (Bio-Rad). Equal amount of protein lysates were  
937 separated by SDS-PAGE, transferred to PVDF membrane, and subjected to  
938 immunoblot analysis for the indicated primary antibodies. Proteins were visualized  
939 using the ECL detection system (Pierce) with the appropriate secondary antibodies.

940

## 941 **Histology**

942 Liver tissues were fixed for 48 h at RT in 10% neutral-buffered formalin (NBF),  
943 dehydrated, embedded in paraffin blocks and sectioned at 7 $\mu$ m. Sections stained  
944 with Masson's Trichrome were examined by light microscopy.

945

## 946 **Statistical analysis**

947 Statistical analyses were performed using GraphPad Prism software (version 6.07).  
948 Fluorescence intensity (Collagen I) was normalized to the number of cells detected  
949 in the field and recorded for 7 fields per well. Cells expressing ACTA2 were  
950 quantified and the percentage of activated fibroblasts (ACTA2<sup>+ve</sup>) was determined for  
951 each field. P values were corrected for multiple testing according to Dunnett's (when  
952 several experimental groups were compared to one condition), Tukey (when several  
953 conditions were compared to each other within one experiment), Sidak (when  
954 several conditions from 2 different genotypes were compared to each other).  
955 Analysis for two parameters (antibody efficacy across time) for comparison of two  
956 different groups were performed by two-way ANOVA. The criterion for statistical



957 significance was  $P < 0.05$ .

958

### 959 **Data Availability**

960 High-throughput sequencing data generated for this study can be downloaded from  
961 the (GEO) repository (data currently under submission). All other data are in the  
962 manuscript or in the supplementary materials.

963

### 964 **References**

- 965 1. Yata, Y. DNase I–hypersensitive sites enhance  $\alpha 1(I)$  collagen gene  
966 expression in hepatic stellate cells. *Hepatology* **37**, 267–276 (2003).
- 967 2. Schafer, S. *et al.* IL-11 is a crucial determinant of cardiovascular fibrosis.  
968 *Nature* **552**, 110–115 (2017).
- 969 3. Cook, S. *et al.* IL-11 is a therapeutic target in idiopathic pulmonary fibrosis.  
970 (2018). doi:10.1101/336537
- 971 4. Myszka, D. G. Improving biosensor analysis. *J. Mol. Recognit.* **12**, 279–284  
972 (1999).
- 973 5. Dou, C. *et al.* P300 Acetyltransferase Mediates Stiffness-Induced Activation  
974 of Hepatic Stellate Cells Into Tumor-Promoting Myofibroblasts.  
975 *Gastroenterology* **154**, 2209–2221.e14 (2018).
- 976 6. Bolger, A. M., Lohse, M. & Usadel, B. Trimmomatic: a flexible trimmer for  
977 Illumina sequence data. *Bioinformatics* **30**, 2114–2120 (2014).
- 978 7. Dobin, A. *et al.* STAR: ultrafast universal RNA-seq aligner. *Bioinformatics* **29**,  
979 15–21 (2013).
- 980 8. Liao, Y., Smyth, G. K. & Shi, W. The Subread aligner: fast, accurate and  
981 scalable read mapping by seed-and-vote. *Nucleic Acids Res.* **41**, e108  
982 (2013).
- 983 9. Love, M. I., Huber, W. & Anders, S. Moderated estimation of fold change and  
984 dispersion for RNA-seq data with DESeq2. *Genome Biol.* **15**, 550 (2014).
- 985 10. Subramanian, A. *et al.* Gene set enrichment analysis: a knowledge-based  
986 approach for interpreting genome-wide expression profiles. *Proc. Natl. Acad.*  
987 *Sci. U. S. A.* **102**, 15545–15550 (2005).
- 988 11. Liberzon, A. *et al.* Molecular signatures database (MSigDB) 3.0.  
989 *Bioinformatics* **27**, 1739–1740 (2011).
- 990 12. Sheng, J., Ruedl, C. & Karjalainen, K. Most Tissue-Resident Macrophages  
991 Except Microglia Are Derived from Fetal Hematopoietic Stem Cells. *Immunity*  
992 **43**, 382–393 (2015).
- 993 13. Chew, V. *et al.* Delineation of an immunosuppressive gradient in  
994 hepatocellular carcinoma using high-dimensional proteomic and  
995 transcriptomic analyses. *Proc. Natl. Acad. Sci. U. S. A.* **114**, E5900–E5909  
996 (2017).